REPORT DOCUMENTATION PAGE

OMB No. 0704-0188

1. REPORT DATE *(DD-MM-YYYY)*	2. REPORT TYPE	3. DATES COVERED (From – To)
28 Nov 06	Final Technical Report	1 Feb 06-30 Nov 09

4. TITLE AND SUBTITLE
Near Net Shape, Ultra High Melting, Erosion Resistant Carbide Metal Composites with Tailored Fibrillar Microstructures via the Displacive Compensation of Porosity Process

5a. CONTRACT NUMBER

5b. GRANT NUMBER
FA9550-07-1-0115

5c. PROGRAM ELEMENT NUMBER

6. AUTHOR(S)
Kenneth H. Sandage, George Institute of Technology

5d. PROJECT NUMBER

5e. TASK NUMBER

5f. WORK UNIT NUMBER

7. PERFORMING ORGANIZATION NAME(S) AND ADDRESS(ES)
Kenneth H. Sandhage
School of Materials Science and Engineering
Georgia Institute of Technology
Atlanta, GA 30332

8. PERFORMING ORGANIZATION REPORT NUMBER

9. SPONSORING/MONITORING AGENCY NAME(S) AND ADDRESS(ES)
USAF/AFRL
AFOSR
875 North Randolph Street
Arlington VA 22203

10. SPONSOR/MONITOR'S ACRONYM(S)
AFOSR

11. SPONSORING/MONITORING AGENCY REPORT NUMBER
AFRL-OSR-VA-TR-2013-1020

12. DISTRIBUTION AVAILABILITY STATEMENT

Distribution Statement A: Approved for public release. Distribution is unlimited.

13. SUPPLEMENTARY NOTES

14. ABSTRACT
The proposed work is of significant importance to the Air Force structural materials program and will result in the understanding of novel advanced materials that are very high melting, lightweight, mechanically robust, and resistant to thermal shock. These materials are needed to significantly enhance the performance of key components in advanced jet and rocket engines, such as nozzles, valves, combustion liners, and thermal exhaust components. Among the most aggressive high-temperature environments encountered in aerospace applications exists in the throat region of a solid-fueled rocket nozzle. Nozzles used with solid, aluminum-bearing fuels are exposed to supersonic impacts of molten aluminum oxide droplets at temperatures in excess of 2500°C. In addition to wear resistance, nozzle materials need to possess a low vapor pressure at such elevated temperatures and should exhibit good creep resistance. Owing to the rapid rise in temperature upon ignition, such nozzles must also be highly resistant to thermal shock and should possess a low coefficient of thermal expansion. For rocket nozzles and other advanced aerospace components, high-temperature, wear-resistant composite materials of lower density are desired that can be fabricated in complex and near net shapes without extensive, costly machining. The capability of producing near net-shape composites with tailorable microstructures (i.e., controlled phase contents and phase shapes) is also needed to allow for enhanced thermo mechanical properties.

15. SUBJECT TERMS

Standard Form 298 (Rev. 8-98)
Prescribed by ANSI-Std Z39-18

Near Net-Shape, Ultra High Melting, Erosion Resistant Carbide/Metal Composites with Tailored Fibrillar Microstructures via the Displacive Compensation of Porosity Process

Contract No. FA9550-07-1-0115

Project Period: Feb. 1, 2007 to May 31, 2010

Final Project Report

Submitted by: *Kenneth H. Sandhage*

Kenneth H. Sandhage
B. Mifflin Hood Professor
School of Materials Science and Engineering
Adjunct Professor, School of Chemistry and Biochemistry
Georgia Institute of Technology
Atlanta, GA 30332
Phone: (404) 894-6882
E-mail: ken.sandhage@ msc.gatech.edu

20130918393

-1-

Abstract:

This 40 month effort has led to four major accomplishments: i) integration of rapid-prototyping approaches (i.e., computer numerical-controlled machining or three-dimensional printing to form shaped, porous WC preforms) with the reactive-infiltration-based Displacive Compensation of Porosity (DCP) process to generate dense, ultra-high-melting, ZrC/W-based composites with tailored, three-dimensional shapes and with near net dimensions (i.e., with dimensional changes, upon conversion of shaped porous WC preforms to dense ZrC/W composites, below 1%), ii) development of gas/solid reaction approaches for converting carbon fibers into tungsten and tungsten carbide fibers, iii) incorporation of such tungsten carbide fibers into shaped porous preforms and then conversion of such preforms, via the DCP process, into dense ZrC/W-based composites that possess fibrillar microstructures, and iv) evaluation of the kinetic mechanism associated with the conversion of porous WC preforms into dense HfC/W-based composites via the DCP process (i.e., solid-state diffusion of carbon through the tungsten lattice and/or through hafnium carbide grain boundaries).

I. Background

Metal/ceramic composites can provide significant improvements in mechanical performance, (e.g., fracture toughness, erosion resistance, and thermal shock resistance) relative to monolithic ceramics.[1-4] A variety of techniques have been used to fabricate metal/ceramic composites, including hot pressing or hot isostatic pressing, plasma spraying, chemical vapor infiltration, and reactive melt infiltration.[5-9] In the latter case, reactions between a porous preform and an infiltrating liquid can broadly be classified as either additive or displacive. While additive reactions tend to be volume expansive (e.g., the conversion of C preforms into Si/SiC composites by the reactive infiltration of molten Si[10]), such reactions are often incapable of generating metal/ceramic composites with operating temperatures that greatly exceed the reactive infiltration temperature (i.e., due to the presence of an appreciable amount of residual solidified metal infiltrant). By contrast, displacive reactions can generate metal phases whose melting points significantly exceed the reactive infiltration temperature. Many embodiments of reactive melt infiltration processes (also called reactive casting) feature solid volume reducing displacive reactions.[11] However, the reactive melt infiltration approach explored in the present work, the patented Displacive Compensation of Porosity (DCP) process[12-14], can generate a larger solid product volume than the volume of solid reactant consumed, resulting in reaction-induced densification.[15,16]

The DCP process has been under investigation in this effort as a means of synthesizing composites for use in extreme, ultra-high temperatures (UHT) environments, such as for solid-fueled rocket motors that must operate at $\geq 2500°C$ under supersonic impingement by molten combustion products.[17,18] Such motor materials must exhibit exceptional UHT erosion and thermal shock resistance.[17,18] In this effort, the DCP process has been examined for generating ultra-high melting refractory metal/carbides. For example, ZrC/W-bearing composites have been created by the infiltration of zirconium-bearing liquids into porous WC preforms via the reaction:

$$\{Zr\} + WC \leftrightarrow W + ZrC \tag{1.1}$$

where $\{Zr\}$ denotes zirconium as a reactive component of the infiltrating liquid. Pure zirconium melts at approximately 1850°C.[19] In order to conduct reactive DCP infiltration at much lower temperatures, zirconium alloy compositions with modest melting points must be used. One such promising alloy system is Cu-Zr. In particular, the compound Zr_2Cu melts congruently at 1025°C.[19] With such Zr-Cu melts, reaction (1.1) is strongly favored from a thermodynamic perspective. Indeed, it has been estimated from available thermodynamic data that reaction (1.1) can spontaneously occur in at 1100-1400°C if the concentration of Zr in the Zr-Cu melt exceeds 920 ppm.[16] Reaction (1.1) is of the DCP (solid volume increasing) type. The solid volume change, Z, associated with this reaction (defined as the change in solid volume upon conversion of WC to ZrC + W divided by the initial WC volume) is +100.8%. The minimum pore volume fraction, Ψ, required to accommodate this solid volume change upon the complete reaction of a rigid preform containing a WC volume fraction, f, can be calculated as:

$$\Psi = \frac{Zf}{1 + Zf} \tag{1.2}$$

For a preform containing only WC (i.e., no inert ZrC or W), $f = 1$, $Z = 1.008$ and $\Psi = 50.2\%$.

-3-

The W/ZrC system possesses an attractive combination of thermochemical and thermomechanical characteristics. For example, the C-W-Zr phase diagram (**Figure 1** below) reveals that a tie line exists between W and ZrC, which indicates that no intermediate compounds can form by the reaction of W with ZrC. Furthermore, the mutual solid solubilities of W in ZrC and ZrC in W are quite limited even at the eutectic melting temperature of 2800°C (7 at.% W soluble in ZrC).[20] Additionally, W and ZrC possess similar coefficients of thermal expansion (CTE) (see **Table 1**).[22,23] The relatively high hardness and low density of ZrC are expected to enhance erosion resistance and provide weight savings for a ZrC/W composite relative to monolithic W, whereas the presence of ductile W at elevated temperatures is expected to improve the fracture toughness of such a composite relative to monolithic ZrC.
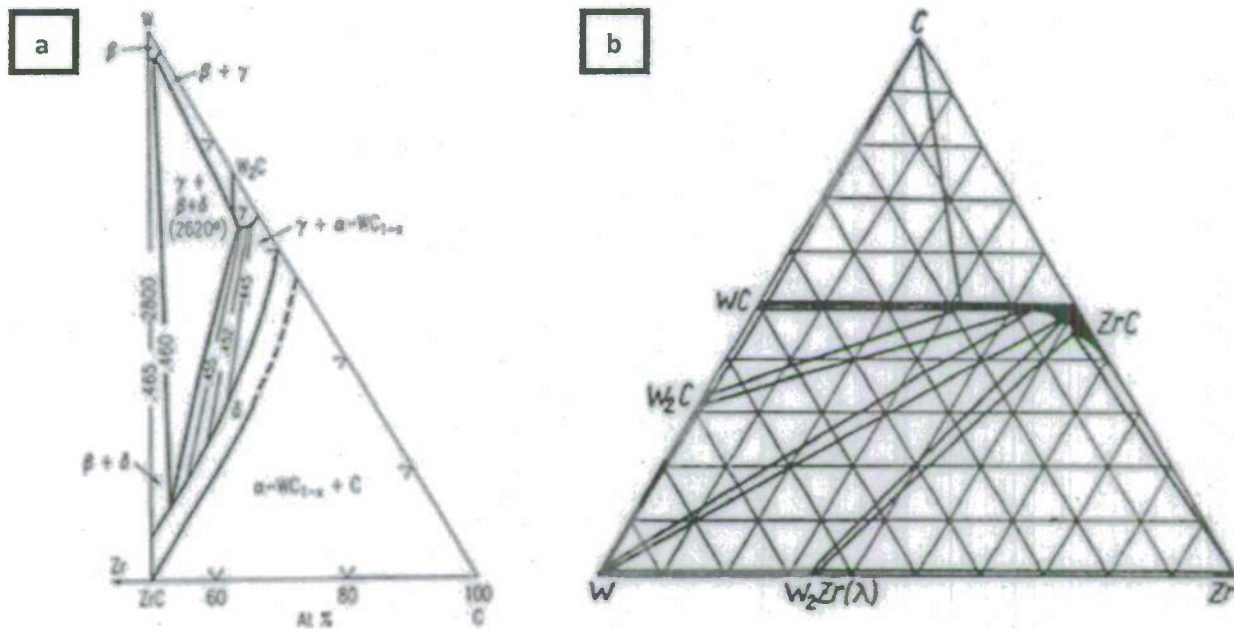

Figure 1. Ternary phase diagrams for the C-W-Zr system: (a) a pseudo-binary projection and (b) an isothermal section at 1500°C.[20,21]

Table 1. Thermomechanical properties of W and ZrC.

Property	W	ZrC
CTE[22,23] @ 25°C [1/°C]	4.5×10^{-6}	4.0×10^{-6}
CTE[22,23] @ 2700°C [1/°C]	9.2×10^{-6}	10.2×10^{-6}
Melting point[24] [°C]	3680	3445
Density[25] [g/cm³]	19.259	6.633
Hardness[26,27] [kg/mm²]	360	2900

II. Integration of Rapid Preform Prototyping with the Displacive Compensation of Porosity (DCP) Process

(as reported in: Lipke, D.W., Zhang, Y., Liu, Y., Church, B.C. and Sandhage, K.H. "Near net-shape/net-dimension ZrC/W-based composites with complex geometries via rapid prototyping and Displacive Compensation of Porosity," *J. Euro. Ceram. Soc.*, 30 (11), 2265-2277 (2010) and Sandhage, K. H. "Materials 'Alchemy': Shape-preserving Chemical Transformation of Micro-to-Macroscopic 3-D Structures," *JOM*, **62** [6] 32-43 (2010).)

Two rapid prototyping methods have been examined for the syntheses of shaped, porous WC preforms: computer numerical-controlled (CNC) machining of rigid, porous WC cylinders, and three-dimensional (3-D) printing. Both approaches have yielded defect-free parts with controlled pore volume fractions, as described below. Microstructural features generated by each preform fabrication method, that are subsequently retained in the produced ZrC/W composites, are also discussed.

Partially-sintered (necked), rigid, porous WC preforms free of residual carbon in the shapes of crucibles, nozzles, and cones were fabricated via CNC machining. These preforms were then immersed in molten Zr_2Cu to allow for reactive conversion into dense ZrC/W-bearing composites. Images of the machined porous WC preforms, as-infiltrated/reacted composites, and cleaned ZrC/W-based composites (with excess residual adherent metal removed) are shown in **Figures 2-4** below.
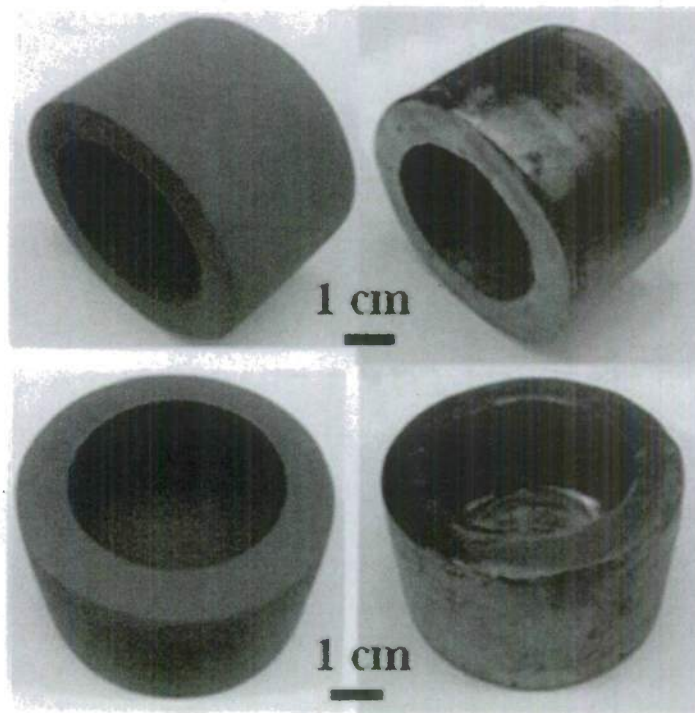

Figure 2. Optical images of: (left) a CNC-machined, crucible-shaped, porous WC preform, (right) a crucible-shaped, near net-dimension, ZrC/W-based composite generated from the same preform by DCP reactive infiltration (after light surface polishing to remove residual adherent solidified copper).
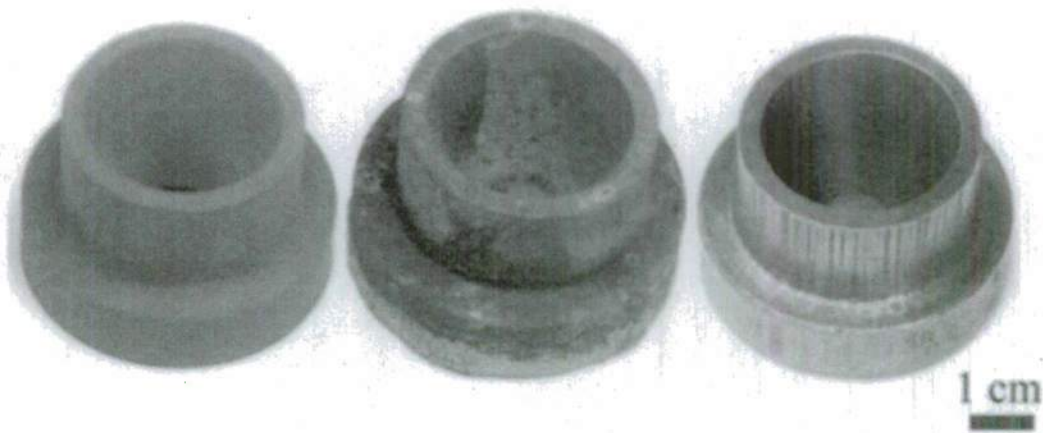
Figure 3. Optical images of: (left) a CNC-machined, nozzle-shaped, porous WC preform, (middle) a nozzle-shaped ZrC/W-based composite generated from the same preform by DCP reactive infiltration (with residual solidified copper still attached), and (right) the nozzle-shaped, near net-dimension ZrC/W-based composite nozzle after light surface polishing to remove residual adherent solidified copper.

Figure 4. Optical images of: (left) a CNC-machined, cone-shaped, porous WC preform, (right) a cone-shaped, near net-dimension ZrC/W-based composite generated from the same preform by DCP reactive infiltration (after light surface polishing to remove residual adherent solidified copper).
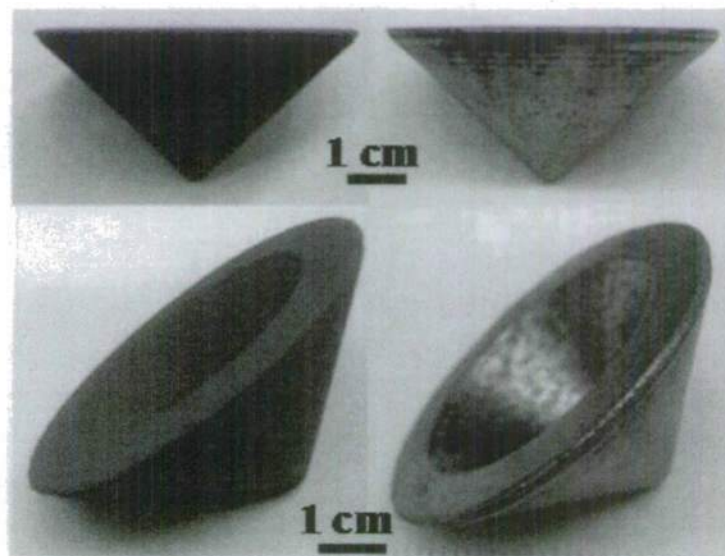
Tungsten carbide preforms in the shapes of nozzles were also fabricated via 3-D printing and subsequently immersed in molten Zr_2Cu to produce W/ZrC-bearing composites. Images of these specimens at various stages of conversion are shown in **Figure 5** below.

Figure 5. Optical images of: (left) a 3-D printed, nozzle-shaped, porous WC preform, (middle) a nozzle-shaped ZrC/W-based composite generated by DCP reactive infiltration (with residual solidified copper still attached), and (right) a nozzle-shaped, near net-dimension ZrC/W-based composite nozzle after light surface polishing to remove residual adherent solidified copper.

Dimensional measurements obtained for the porous WC preforms and for the final ZrC/W-bearing composites (after removal of residual adherent copper) are listed in **Table 2** below.

Table 2. Dimension measurements of starting porous WC preforms and of the resulting dense DCP-derived ZrC/W-based composites.

Geometrical Feature	Ave. Dimension of WC Preform [mm]	Ave. Dimension of W/ZrC Composite [mm]	% Change
CNC machined nozzle			
OD nozzle exit	50.65 ± 0.09	50.32 ± 0.16	-0.65%
OD nozzle entrance	37.50 ± 0.08	37.23 ± 0.07	-0.72%
Nozzle height	32.13 ± 0.22	32.00 ± 0.30	-0.40%
CNC machined cone			
Bottom diameter	52.40 ± 0.08	51.98 ± 0.15	-0.80%
Cone height	26.03 ± 0.05	25.87 ± 0.07	-0.61%
CNC machined crucible			
Outer diameter	55.62 ± 0.07	55.19 ± 0.05	-0.77%
Inner diameter	36.71 ± 0.08	36.44 ± 0.09	-0.74%
Outer height	35.20 ± 0.07	35.00 ± 0.06	-0.57%
Inner height	24.34 ± 0.06	24.22 ± 0.05	-0.49%
3D printed nozzle			
OD nozzle exit	54.23 ± 0.25	53.90 ± 0.12	-0.61%
OD nozzle entrance	40.34 ± 0.20	40.09 ± 0.13	-0.62%
Nozzle height	34.82 ± 0.15	34.53 ± 0.23	-0.83%

The images in **Figures 2-5** and the data in **Table 2** confirm the 3-D shape and dimension preservation (to within less than 1%) of the ZrC/W-based composites generated by application of the DCP process to the CNC-machined or 3-D printed (rapid prototyped) WC preforms. In addition to bulk 3-D shape preservation, fine surface features present on the WC preforms (e.g., milling features) were also preserved in the DCP-converted, ZrC/W-based composites. For example, the vertical striations introduced by CNC milling to the shaped, porous WC preforms were retained on the external surfaces of the final ZrC/W-based composites (see the rightmost image in **Figure 3**).

In order to evaluate the extent of conversion of WC preforms into ZrC/W composites upon reactive infiltration, the phase contents of reacted specimens were characterized by measurements of weight and dimension changes and via quantitative XRD analyses. For the latter analyses, calibration curves were generated to quantitatively correlate XRD peak areas to the actual phase contents present in known mixtures. **Figure 6** reveals diffraction patterns obtained from standard mixtures corresponding to (front-to-back) 70, 80, 90, and 95% conversion of WC into W + ZrC (i.e., the mixtures were prepared in stoichiometries consistent with varied amounts of reaction (1.1)). The peaks in the displayed range correspond to (left-to-right): the (001) diffraction peak of WC, the (111) diffraction peak of ZrC, the (100) diffraction peak of WC, the (200) diffraction peak of ZrC, the (110) diffraction peak of W. The peak area ratios of the 100% intensity peaks for W (the (110) peak) and for WC (the (100) peak) were then plotted as a function of the equivalent extent of conversion (**Figure 7**). The XRD data obtained from reactively-infiltrated specimens was fitted to the equation:

$$y = \frac{KX}{1 - X} \tag{1.3}$$

where y is the W:WC peak area ratio, K is a fitted parameter (0.5966), and X is the extent of reaction (the molar ratio of W:WC being $X/(1-X)$). The extent of reaction was related to the
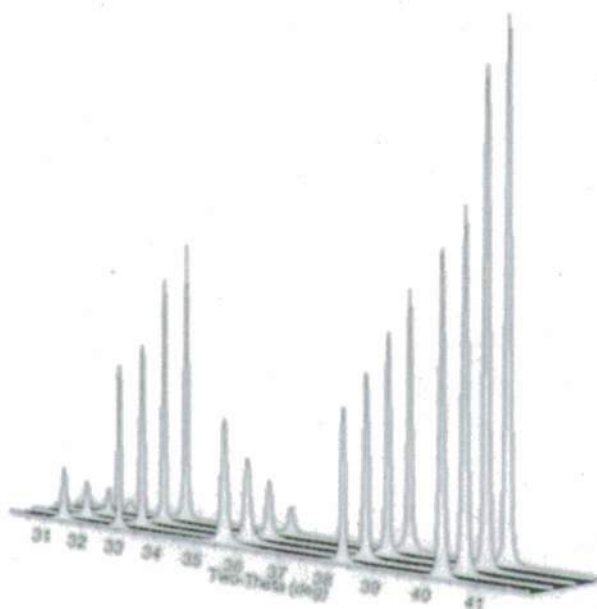

Figure 6. Representative XRD spectra used to generate the calibration curve in Figure 7 below.
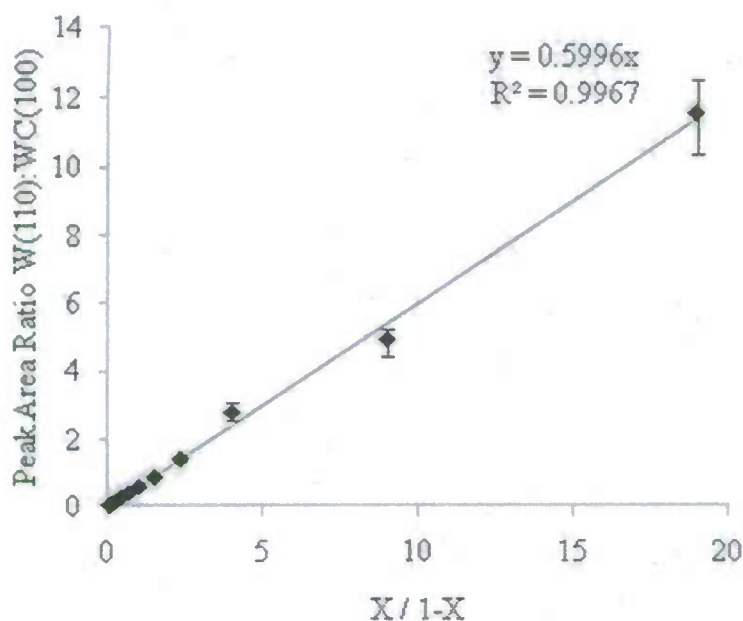
Figure 7. XRD calibration curve.

measured W(110):WC(100) peak-area-ratios by the equation:

$$X = \frac{y}{y + K} \tag{1.4}$$

Although it was also possible to construct a calibration curve utilizing ZrC(111):WC(100) peak area ratios, the relatively small observed peak intensities of ZrC versus W (due to differences in atomic scattering factors) resulted in greater susceptibility to error from profile fitting, so only calibration curves utilizing the W:WC peak ratio were used for quantitative phase analyses.

XRD analysis of a polished cross-section of a 3-D printed and DCP-infiltrated W/ZrC-bearing composite yielded an average W:WC peak area ratio of 12.5:1, which corresponded to a molar ratio of 21:1 W:WC. Physical data used for further quantitative calculation of the phase content (including for the amounts of ZrC and Cu) are listed in **Table 3** below.

Table 3. Molar volumes of reactant and product phases involved in the DCP reaction of Zr_2Cu liquid with porous WC preforms.

Phase		Molar Weight [g/mol]	Density [g/cm³]	Molar Volume [cm³/mol]
WC		195.861	15.667	12.502
W		183.85	19.259	9.546
ZrC		103.231	6.633	15.563
Cu		63.546	8.932	7.114
Liquids @ 1100°C	Cu(l)	63.546	7.99	7.96
	Zr_2Cu(l)	81.998	6.77	12.11

Quantitative XRD analyses coupled with weight change and dimensional change measurements, along with the data in **Table 3**, have been used to calculate the phase contents and theoretical

densities of composites produced via combination of rapid prototyping and DCP processing. As shown in **Tables 4-6**, the porous WC preforms were converted to a high degree (90-95%) into ZrC/W-based composites of low porosity (94-100% of theoretical density) by the DCP process.

Table 4. Phase content of a DCP-derived ZrC/W-based composite generated by the reactive infiltration of $Zr_2Cu(l)$ into a porous WC preform.

WC Preform* ρ [g/cm^3]	ZrC/W-based Composite ρ [g/cm^3]		Extent of Reaction (Vol. %)	
7.47 ± 0.01	10.99 ± 0.05		92 ± 1	
Phase Contents (Vol. %)				
ZrC	W	Cu	WC	Pore
54 ± 6	33 ± 4	9 ± 1	5 ± 1	-1 ± 7

*This WC preform was prepared by the compaction of a mixture of WC powder with a rice starch binder, pyrolysis of the binder, and then partial sintering at 1450°C for 4 h.

Table 5. Phase content of a DCP-derived ZrC/W-based composite generated by the reactive infiltration of $Zr_2Cu(l)$ into a porous WC preform.

WC Preform* ρ [g/cm^3]	ZrC/W-based Composite ρ [g/cm^3]		Extent of Reaction (Vol. %)	
7.25 ± 0.01	11.61 ± 0.05		90 ± 1	
Phase Contents (Vol. %)				
ZrC	W	Cu	WC	Pore
54 ± 6	33 ± 4	5 ± 1	4 ± 1	4 ± 7

*This WC preform was prepared by the compaction of a mixture of WC powder with an ammonium acetate binder, pyrolysis of the binder, and then partial sintering at 1450°C for 4 h.

Table 6. Phase content of a DCP-derived ZrC/W-based composite generated by the reactive infiltration of $Zr_2Cu(l)$ into a porous WC preform.

WC Preform* ρ [g/cm^3]	ZrC/W-based Composite ρ [g/cm^3]		Extent of Reaction (Vol. %)	
6.63 ± 0.01	10.58 ± 0.05		95 ± 1	
Phase Contents (Vol. %)				
ZrC	W	Cu	WC	Pore
51 ± 6	32 ± 4	9 ± 1	2 ± 1	6 ± 7

*This WC preform was prepared by the 3-D Printing of WC powder with a polyethyleneimine/glycerol binder, pyrolysis of the binder, and then partial sintering at 2100°C for 4 h.

Microstructural features present in the starting porous preforms were also retained in the DCP-derived composites. Prior work[28] has indicated that the reaction of WC with $Zr_2Cu(l)$ proceeds by the formation of conformal layers of ZrC and W on the reacting WC. Hence, the morphology of the reactant WC phase was expected to have a strong influence on the morphologies of the ZrC and W product phases. Secondary and backscattered electron images, and energy-dispersive x-ray analyses, of polished cross-sections of DCP-derived composites generated from CNC-machined and 3-D printed preforms are shown in **Figures 8 and 9**,
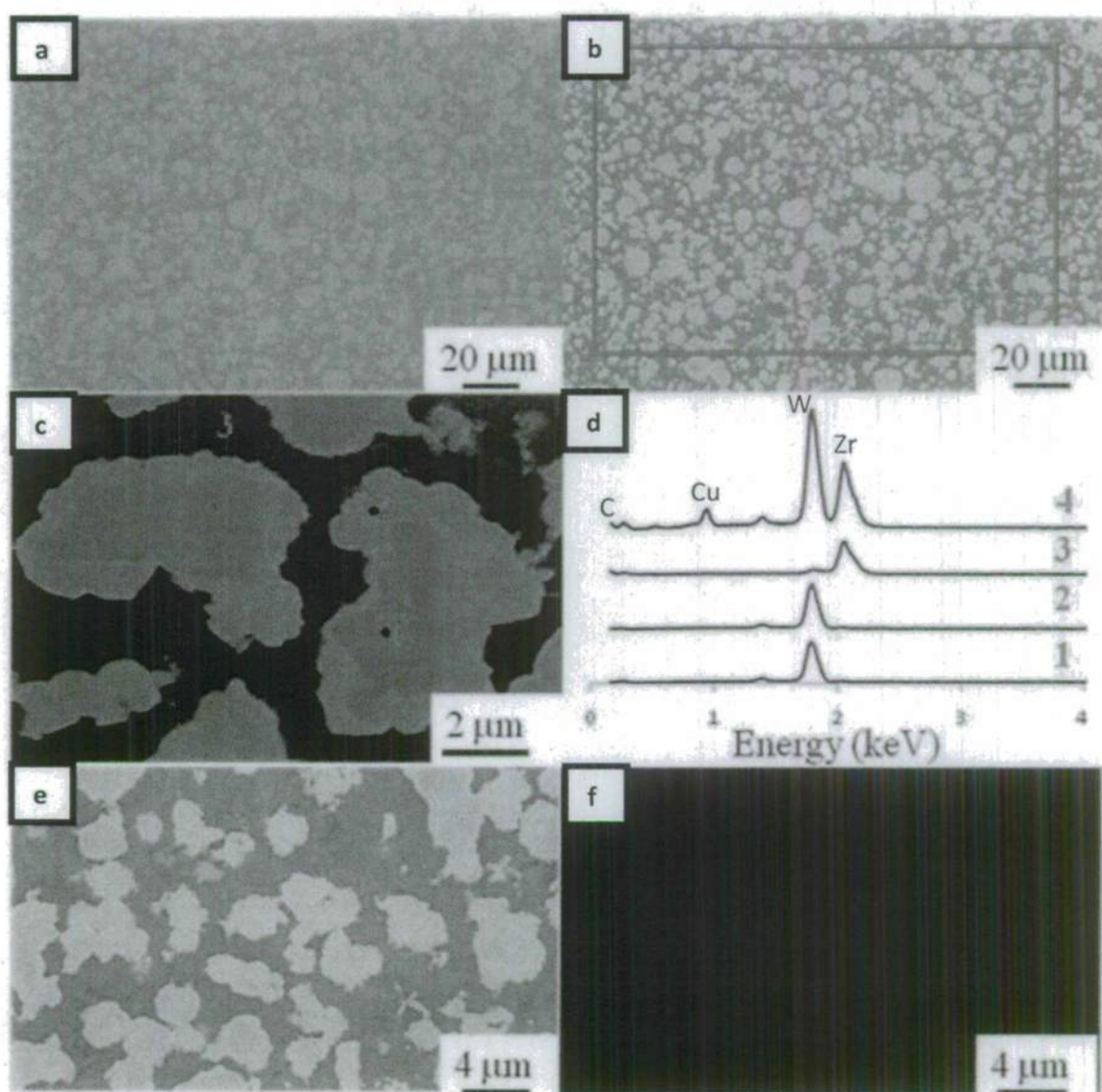

Figure 8. Microstructural analyses of polished cross-sections of a ZrC/W-based composite generated via the reactive infiltration of a CNC-machined porous WC preform with $Zr_2Cu(l)$: (a) secondary electron (SE) image, (b), (c) backscattered electron (BSE) images, (d) energy-dispersive x-ray (EDX) spectra obtained at the locations indicated in (b) and (c), and (e), (f) BSE image and associated EDX map, respectively, for tungsten (in blue) and zirconium (in red).
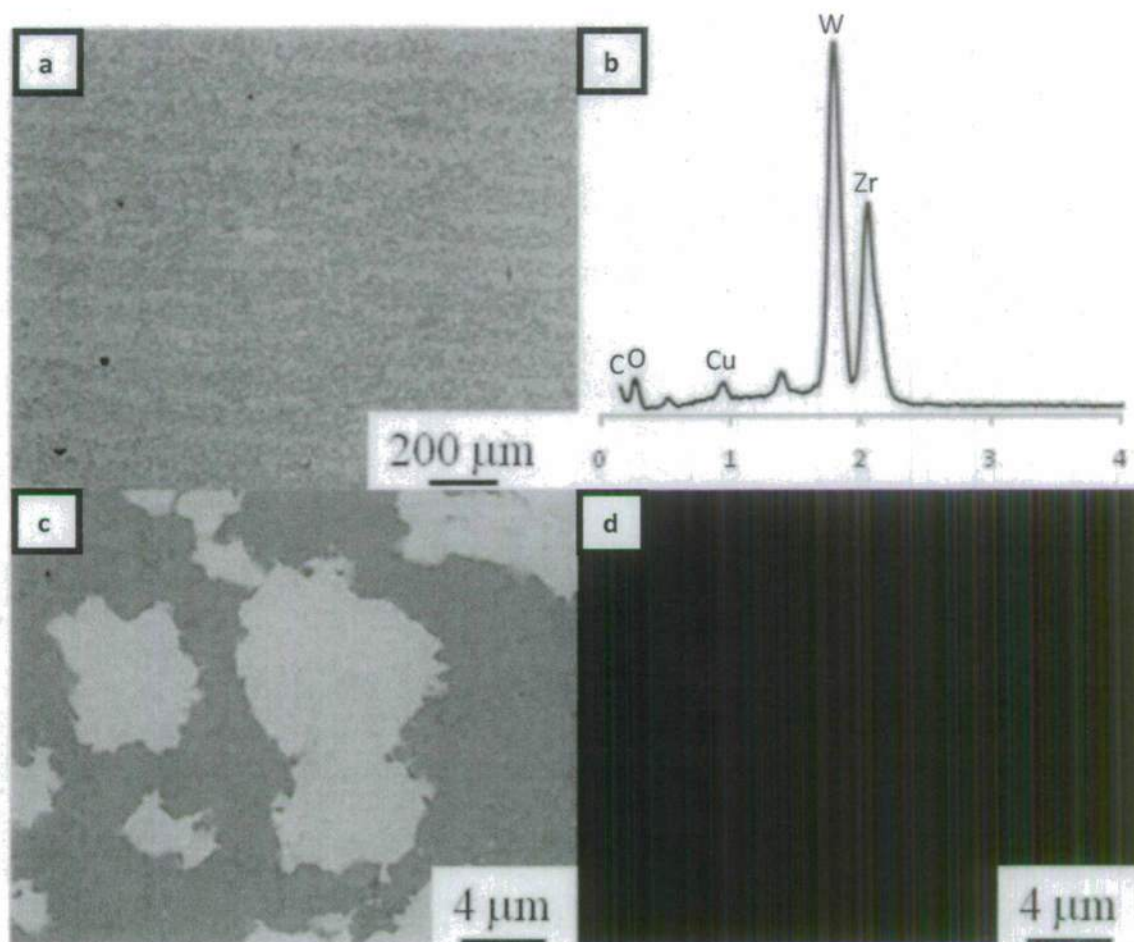
Figure 9. Microstructural analyses of polished cross-sections of a ZrC/W-based composite generated via the reactive infiltration of a 3-D-printed porous WC preform with $Zr_2Cu(l)$: (a) BSE image, (b) energy-dispersive x-ray (EDX) spectrum of the composite, and (c), (d) BSE and associated EDX map, respectively, for tungsten (in blue) and zirconium (in red).

respectively. Porous WC preforms prepared by uniaxial compaction, partial sintering, and then CNC machining consisted of relatively random distributions of necked WC powder particles and pores. Consequently, upon reactive infiltration of the rigid porous WC particle-based preforms with $Zr_2Cu(l)$, the more voluminous ZrC and W product phases formed around the WC particles and filled in the prior pore spaces. The resulting composite consisted of a ZrC-bearing matrix (the grey matrix in **Figures 8a and b**; the dark matrix in **Figure 8c**) surrounding W-bearing particles that were distributed in a relatively random and uniform manner. On the other hand, the layer-by-layer 3-D printing process yielded porous WC preforms comprised of WC particle-rich layers. Reactive infiltration of these WC preforms yielded ZrC/W-based composites that retained the laminated morphology of the WC preforms (**Figure 9a**).

WC particle preforms with pore volume fractions less than Ψ (equation (1.2) above) may retain residual WC, in the form of particles with unreacted WC cores surrounded by W and ZrC products, after reactive infiltration with $Zr_2Cu(l)$. Consider, for example, a spherical particle of WC undergoing reaction (1.1). The radial positions of the WC/W interface (r_{WC}) and the ZrC/liquid interface (r_W), are related to the volume extent of reaction, X, by:

-12-

$$\frac{r_{WC}}{r_0} = (1 - X)^{1/3} \qquad (1.5)$$

$$\frac{r_W}{r_0} = \left(1 - X + X\left[\frac{V_W}{V_{WC}}\right]\right)^{1/3} \qquad (1.6)$$

$$\frac{r_{ZrC}}{r_0} = (1 + ZX)^{1/3} \qquad (1.7)$$

where r_0 = original particle radius and V_j = molar volume of phase j. As a WC particle is consumed by reaction, the WC/W interface recedes inward (toward the original WC particle center) while the ZrC/liquid interface migrates outward (**Figure 10**). Calculated values of the ratios r_{WC}/r_0, r_W/r_0, and r_{ZrC}/r_0 at selected values of X are summarized in **Table 7**.
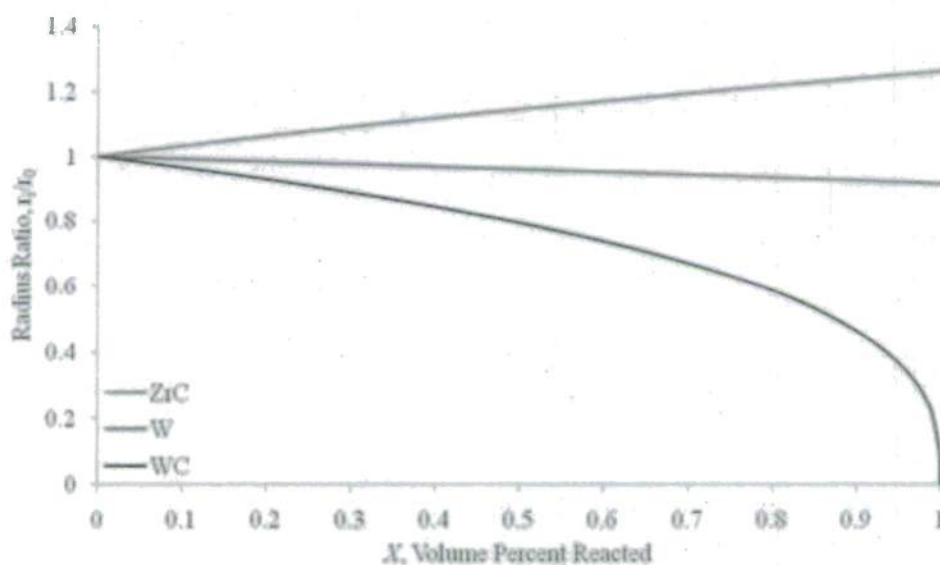

Figure 10. Ratio of the relative radial positions of the WC/W interface (black, r_{WC}/r_0), the W/ZrC interface (blue, r_W/r_0), and the ZrC/liquid interface (red, r_{ZrC}/r_0) as a function of the volume fraction of reacted WC, X.

Table 7. Ratios of the radial positions of the WC/W, W/ZrC, and ZrC/liquid interfaces to the unreacted particle radius (r_{WC}/r_0, r_W/r_0, and r_{ZrC}/r_0, respectively) as a function of the volume percent reacted, X.

X	r_{WC}/r_0	r_W/r_0	r_{ZrC}/r_0
0.80	0.585	0.933	1.218
0.90	0.464	0.923	1.240
0.95	0.368	0.919	1.251
0.99	0.215	0.915	1.260
0.999	0.100	0.914	1.261
0.9999	0.046	0.914	1.262
1	0	0.914	1.262

It is worth noting that, even with extensive reaction, residual WC may be detected in polished cross-sections of ZrC/W-based composites. For example, with 90 vol% conversion of a spherical WC particle, the unreacted WC core radius would comprise 46.4% of the starting WC particle radius. Even with 99.9 vol% conversion, the unreacted WC core radius would comprise 10% of the starting WC particle radius. Hence, it should not be surprising that occasional particles containing some unreacted WC (e.g., **Figure 8c**) were observed in reactively-infiltrated composites that had undergone ≥90 vol% reaction (as evaluated in **Tables 4-6**).

It is unclear to what extent, if any, the presence of unreacted WC cores may have on the performance of W/ZrC-bearing composites produced via the DCP process. W and WC cannot be in equilibrium, and can react to form W_2C at elevated temperatures.[20,21] However, the corresponding reaction to form W_2C is not accompanied by an appreciable volume change. W_2C and WC share similar melting points that are not far from the W-ZrC eutectic temperature (2776°C vs. 2800°C). WC and W_2C are also relatively hard phases.[26] Hence, the presence of some residual WC or W_2C may not prove to be particularly impactful for intended composite applications. The presence of residual Cu in the minor detected quantities of the present work (5-9 vol%) may also not be detrimental. For example, copper has been intentionally introduced to tungsten-based nozzles to allow for transpirational cooling.[17,18]

The DCP process has been shown to be capable of producing near net-shape and near net-dimension ceramic/refractory metal composites via reaction-induced densification of porous ceramic preforms. In the present work, two rapid prototyping techniques, CNC machining and 3-D printing, have been utilized to fabricate porous WC preforms in a variety of 3-D shapes (nozzles, cones, crucibles, etc.). These shaped, porous WC preforms have then been reactively infiltrated with $Zr_2Cu(l)$ to produce dense ZrC/W-based composites (51-54 vol.% ZrC, 32-33 vol.% W, 5-9 vol.% Cu, 2-5 vol.% WC, and 1-7 vol.% pores) that retained the 3-D preform shape and dimensions (to within less than 1%).

III. Conversion of Carbon Fibers and Preforms into Tungsten and Tungsten Carbide

(Lipke, D.W. and Sandhage, K.H. "Porous Refractory Metal Replicas via Reactive Conversion of Carbon Templates" U.S. Provisional Patent Application, GTRC ID 5149 (2010).)

In Section II above, the microstructures of DCP-derived composites (**Figures 8 and 9**) have been shown to be correlated to the microstructures of the starting porous preforms. Preforms fabricated via CNC machining of pressed and partially-sintered WC powder compacts were converted into ZrC/W-based composites with relatively uniform distributions of the ZrC and W phases (consistent with the relatively uniform distributions of WC particles and pores in the preform). However, the DCP conversion of porous WC preforms fabricated by the layer-by-layer 3-D printing process yielded ZrC/W-based composites that retained the laminated microstructure of the preforms. Further optimization of the DCP process may include refined preform fabrication techniques to introduce controlled anisotropy into the microstructure to allow for additional tailoring of the microstructure and properties of the final composites.

The fracture strength and fracture toughness of ceramic matrix composites can be improved by the introduction of ductile metallic reinforcements.[29-31] The degrees by which crack deflection at weak metal/ceramic interfaces and crack bridging by ductile metal reinforcements improve fracture toughness have been shown to vary with both the amount and the contiguity of the reinforcing phase.[29-31] Numerous attempts have been made to create highly interconnected metal carbides (or metal carbide precursors, such as base metals and metal oxides) in the forms of discontinuous fibers and whiskers, continuous fibers and cloths, and as coatings by a wide variety of techniques. For example, chemical vapor deposition has widely been employed using metal halide vapors, hydrogen gas, and hydrocarbon gas or carbon present in or on the substrate to deposit a variety of metal carbides.[32-34] Solution-based processing has yielded contiguous carbides by dissolution of metal chlorides in solvents, impregnation into organic cloths, and subsequent high temperature thermal treatment.[35,36] Sol-gel processing has produced oxide coatings that have been carbothermally reduced and carbidized.[37-39] Molten salts[40] and molten metal alloys[41,42] have been used as flux media for dissolution of reactive metals that subsequently react with carbon to form carbide coatings. Tungsten and tungsten oxide whiskers have been grown via vapor-liquid-solid mechanisms[43], by hydrogen reduction of tungsten oxide[44], and by reaction of tungsten metal powder with nickel nitrate[45], respectively. Complex tungsten compounds have been grown as whiskers, and subsequently reduced and carbidized by thermal treatment in hydrogen/hydrocarbon atmospheres.[46] Some of these techniques require specialized processing equipment[38,48] and present processing challenges preventing their immediate adaptation to the production of contiguous WC preforms (such as cracking and shrinkage[39,40], limited chemistries for tungsten[44,45], and inability to produce thick coatings[41-43,46]).

In order to take advantage of biomorphic carbonaceous templates[47,48] and well-established carbon microfabrication methods, such as polymerization/pyrolyzation[49,50] and chemical vapor infiltration[51], it is desirable to directly and completely convert carbon into metal or metal carbide replicas. While some of these methods take advantage of carbonaceous templates to form coatings, none directly and completely consume the template to form metal or metal carbide replicas. However, two methods[52,53] have been reported to reactively convert high-surface area carbon to carbides via reaction with volatile metal oxide vapors:

$$MO_x(g) + (1 + x)C \leftrightarrow MC + xCO(g) \qquad\qquad (1.8)$$

Such reactions become feasible when sufficient metal oxide vapor pressures are developed at the reaction temperatures. For example, the vapor pressure of silicon monoxide, formed by equilibration of powdered silicon and silicon dioxide, is 7.5×10^{-3} atm at 1400°C and 1 atm total pressure.[54] Similarly, the total vapor pressure of tungsten oxide vapor species, formed over tungsten trioxide powder, is 1.25×10^{-2} atm at 1400°C and 1 atm total pressure (assuming an oxygen partial pressure greater than 6 ppb such that WO_3 is the most stable oxide).[54] However, unlike silicon monoxide vapors, tungsten oxide vapors are highly corrosive and react with refractory ceramic containers such as MgO, ZrO_2, Al_2O_3 and mullite to form eutectic liquids at modest temperatures[55], making safe encapsulation of the carbon-containing article with tungsten oxide vapors challenging.

As a result of difficulties in setting up experimental equipment, initial attempts to convert carbon fibers via reaction with tungsten oxide-based vapors proved unsuccessful. The starting amorphous carbon fibers used in these trials are shown in **Figure 11**. A number of coating and
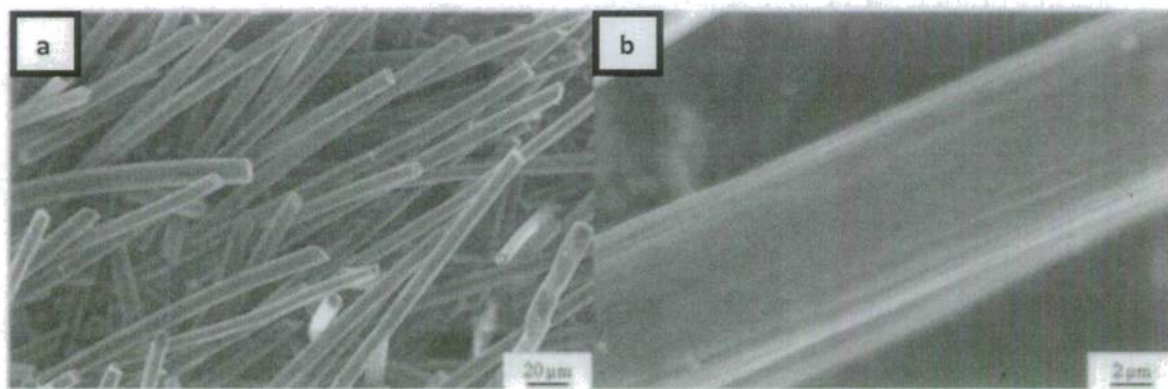

Figure 11. Zoltek panex-30 milled carbon fibers.

conversion techniques were then explored, ranging from gas-solid reactions, to liquid-solid reactions (with oxide and metal alloy-based melts), to solid-solid reactions (with oxide-based coatings). Of these attempts, three may merit further investigation: the reaction of carbon with B_2O_3-WO_3 melts[56], the cathodic electrodeposition of WO_3 from peroxotungstic acid solution[57] onto carbon followed by high temperature solid-state reaction with carbon, and the reaction of tungsten-bearing gases with carbon.

Liquid-solid reaction of carbon fibers with molten B_2O_3-WO_3 at 1100°C produced metallic tungsten coatings on the fibers, as indicated in **Figures 12a and b**. However, carbon dissolution into the melt at this temperature was relatively rapid and resulted in the liberation of significant amounts of detached W particles into the melt and abnormal W grain growth. Modifications of melt chemistry that would increase in the activity of WO_3 in the melt[58] or decrease the carbon solubility, are suggested as potential future directions of research with this approach.

Electrodeposition of WO_3 onto the carbon fibers, followed by solid-solid reaction with the underlying carbon fibers at 1200°C, yielded WC/W-coated fibers as indicated in **Figures 12c and d**. However, this approach was limited by the inability to form thick, coherent, and continuous coatings on the discontinuous fibers, which may have been the result of poor electrical contact with many of the fibers during the electrodeposition process. Interconnected
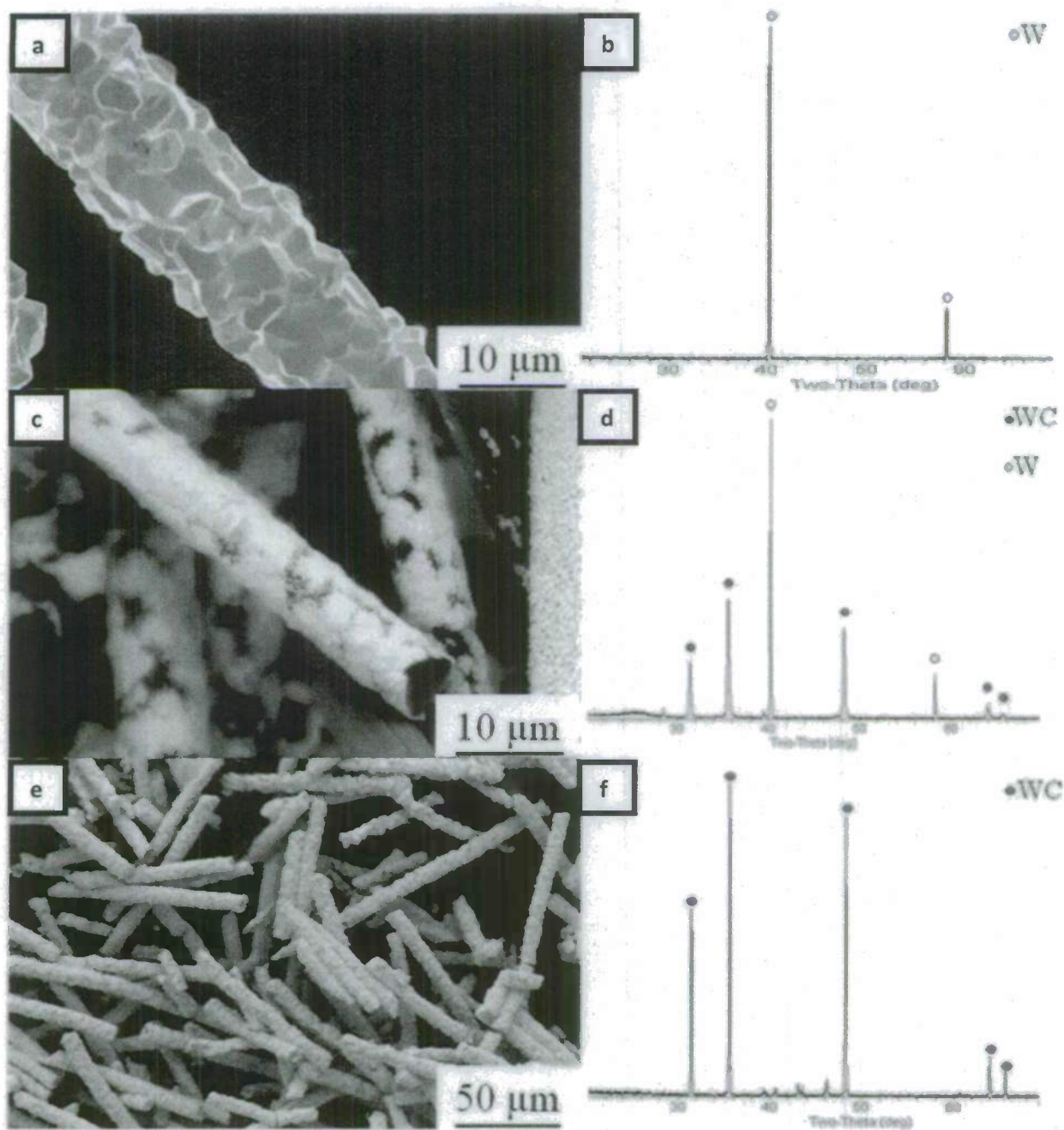
Figure 12. Carbon fiber coating and conversion. (a) SE image and (b) x-ray diffraction (XRD) analysis of carbon fibers after reaction with a B_2O_3-WO_3 melt at 1100°C. (c) SE image and (d) XRD analysis of carbon fibers after reaction with electrodeposited WO_3 at 1200°C; (e) SE image and (f) XRD analysis of carbon fibers after reaction with tungsten chloride vapor at 1400°C.

preforms, rather than discontinuous fibers, may act as conductive, interconnected templates that are more suitable for this method.

The reaction of carbon fibers with tungsten chloride gas at 1400°C yielded tungsten carbide-bearing fibers, as indicated in **Figures 12d and f**. Such tungsten chloride gas was generated by a displacement reaction between molten $CuCl_2$ and W:

$$CuCl_2 + W \leftrightarrow WCl_2(g) + Cu \qquad (1.9)$$

$$2WCl_2(g) + C \leftrightarrow WC + WCl_4(g) \qquad (1.10)$$
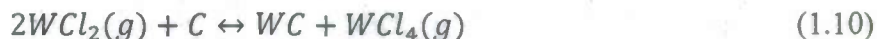
The stoichiometry of reaction (1.10) was especially noteworthy, as a volume expansion of +129.3% should occur upon conversion of solid carbon into tungsten carbide. This reaction-induced increase in solid volume can allow a highly porous carbon preform (61.2% pore volume fraction) to be converted into a less porous WC preform (50.2% pore volume fraction) for subsequent DCP conversion into a dense ZrC/W-based composite.

The reaction of proprietary tungsten-bearing vapor with carbon fibers to yield tungsten fibers has also been examined. A partially-reacted carbon fiber possessing a tungsten cladding on unreacted carbon is shown in **Figure 13**. Such partially-reacted fibers were found to possess an internal pore channel, which was consistent with Kirkendall porosity resulting from relatively rapid outward diffusion of carbon through the tungsten cladding. Fully-converted hollow tungsten fibers are shown in **Figure 14**. No residual carbon cores were detected in these more extensively reacted fibers.
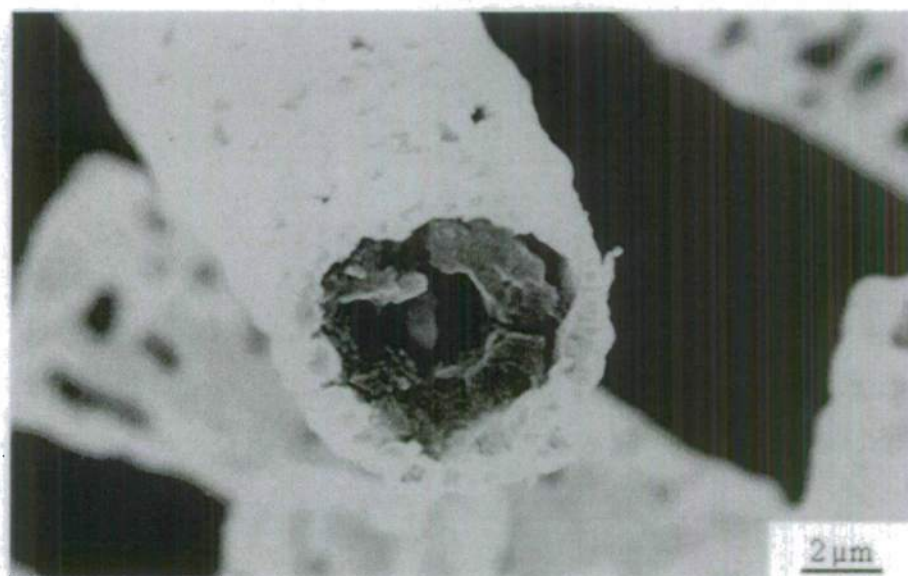

Figure 13. SE image of a partially-reacted fiber showing a continuous bright polycrystalline tungsten cladding, residual unreacted carbon (dark), and an interior pore channel.
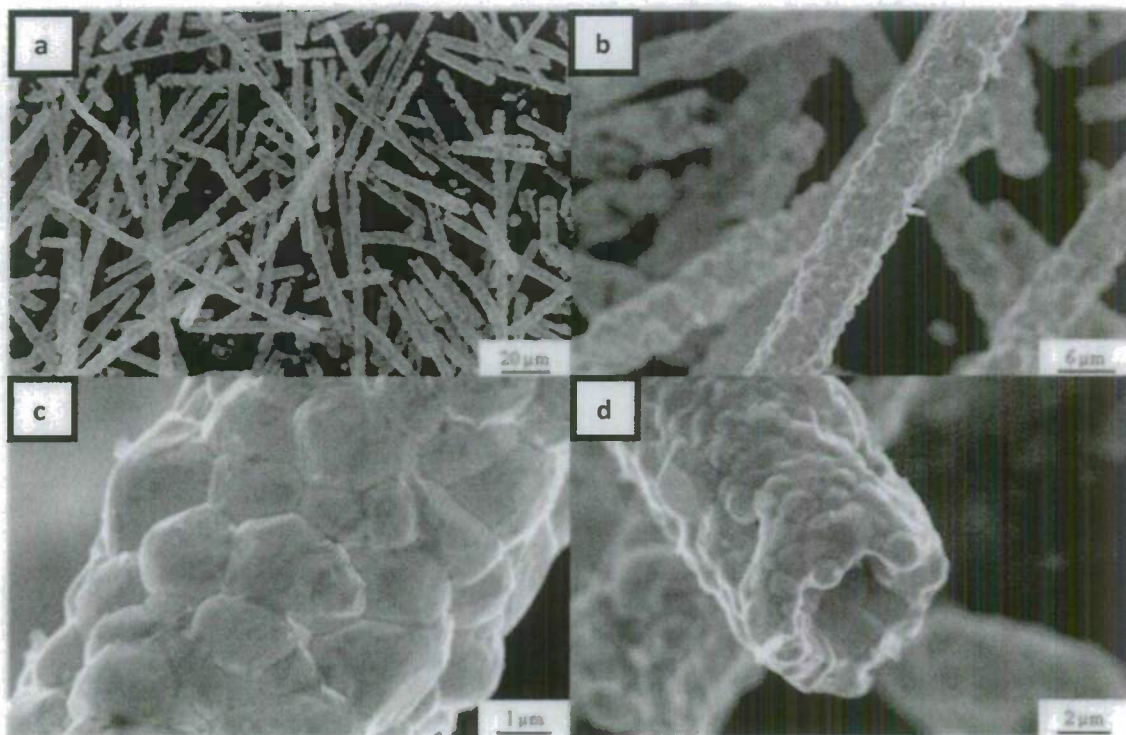
Figure 14. SE images of hollow, polycrystalline tungsten fibers generated via the reaction of carbon fibers with a proprietary tungsten-bearing vapor.
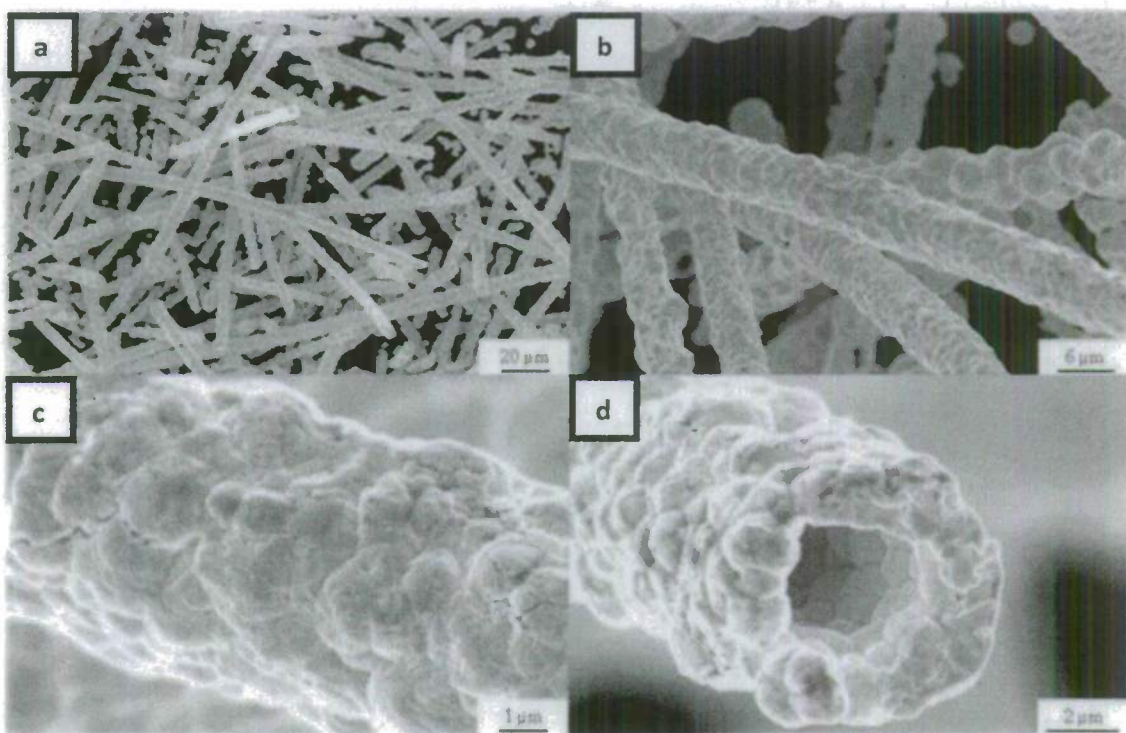

Figure 15. Hollow WC-bearing fibers generated via reaction of hollow W fibers (of the type shown in Figure 14) with CO(g).

These hollow tungsten fibers were then carburized via reaction with CO(g) to generate the polycrystalline WC-based fibers shown in **Figure 15**. XRD analysis confirmed the presence of appreciable WC in these carburized fibers. The measured W(110):WC(100) peak area ratio of 0.079 corresponded to a phase content of 12 mole% W and 88 mole% WC using the calibration method described in Section II.

In addition to fibers, porous graphitic foams were converted into porous tungsten replicas via reaction with the proprietary tungsten-bearing gas, as shown in **Figure 16**. The measured changes in external dimensions were less than 1% after such reactive conversion. Microstructural features of the graphitic carbon foams were also preserved in the polycrystalline tungsten products, as
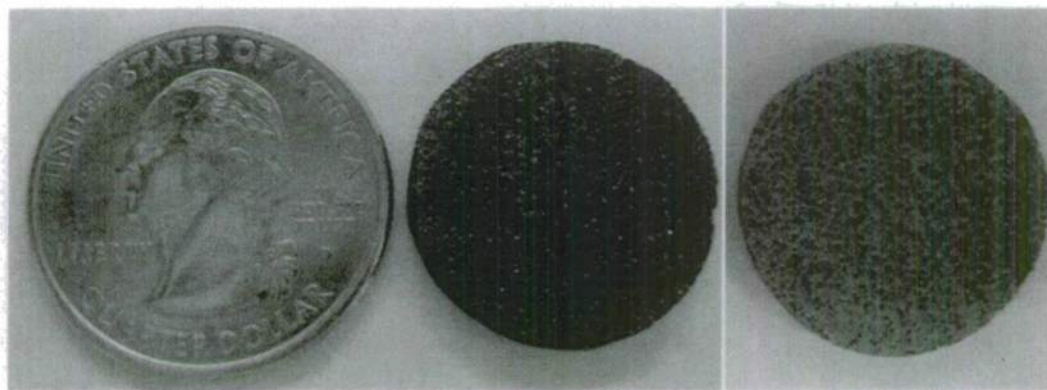

Figure 16. Optical images revealing the conversion of a porous Poco graphitic carbon preform (middle) into a porous tungsten replica (right).

shown in **Figure 17**. Characterization by XRD, EDX, and HRTEM analyses confirmed that no residual carbon phase was present within the reacted foams. The bulk density increased from 0.37 ± 0.01 g/cm^3 for the porous carbon preforms to 1.20 ± 0.01 g/cm^3 for the porous tungsten products. Taking the theoretical bulk densities of graphite as 2.20 g/cm^3 and tungsten as 19.25 g/cm^3, the total porosity of the foam was calculated to decrease from $17 \pm 1\%$ to $6 \pm 1\%$. This decrease was consistent with the expected solid volume change upon reaction.

The morphology-preserving transformation of easily-shaped carbon preforms into tungsten replicas can be an attractive means of fabricating tungsten components for a number of applications, including for solid fueled rocket motors[17], nuclear fusion plasma divertors[59], shaped reinforcements (e,g, hollow fibers) for bulk metallic glass composite kinetic penetrators[60], and for infrared photonic crystals for thermophotovoltaics[61].
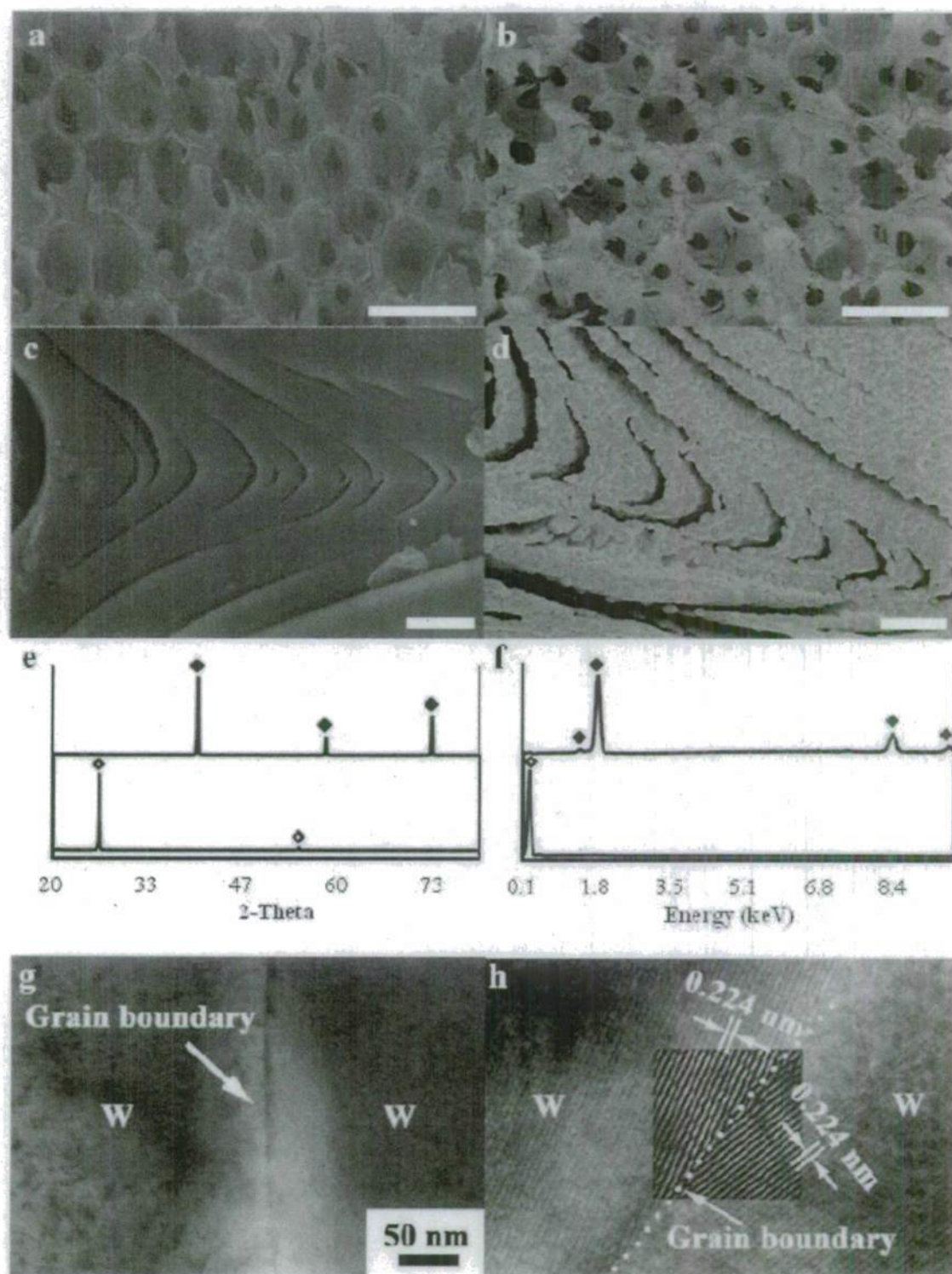
Figure 17. SE images of: (a), (c) as-received Poco HTC graphitic C foam, (b), (d) tungsten-converted replicas. (Scale bars in (a), (b) = 1 mm; scale bars in (c), (d) = 10 μm.) (e) XRD and (f) XPS analyses of (bottom) as-received Poco HTC graphitic C foam and (top) tungsten-converted replicas (◇ Graphitic C, ◆ W); (g) TEM and (h) HRTEM micrographs of tungsten grain boundaries in the converted foams.

IV. DCP Conversion of WC fiber-bearing preforms into ZrC/W-based composites with Fibrillar Microstructures

To demonstrate that the DCP process can be used to generate composites with fiber-shaped phases, hollow tungsten fibers produced by the reaction of carbon fibers with the proprietary tungsten-bearing vapor (as discussed in Section III) were subsequently carbidized (by reaction with CO(g)) and incorporated with WC powder into uniaxially-pressed preforms. After partial sintering, the porous WC specimens were reactively infiltrated with $Zr_2Cu(l)$. Cross-sections of the resulting ZrC/W-based composites are shown in **Figure 18** below. The fibrillar morphology of the hollow WC fibers was preserved in the converted ZrC/W-based composites.
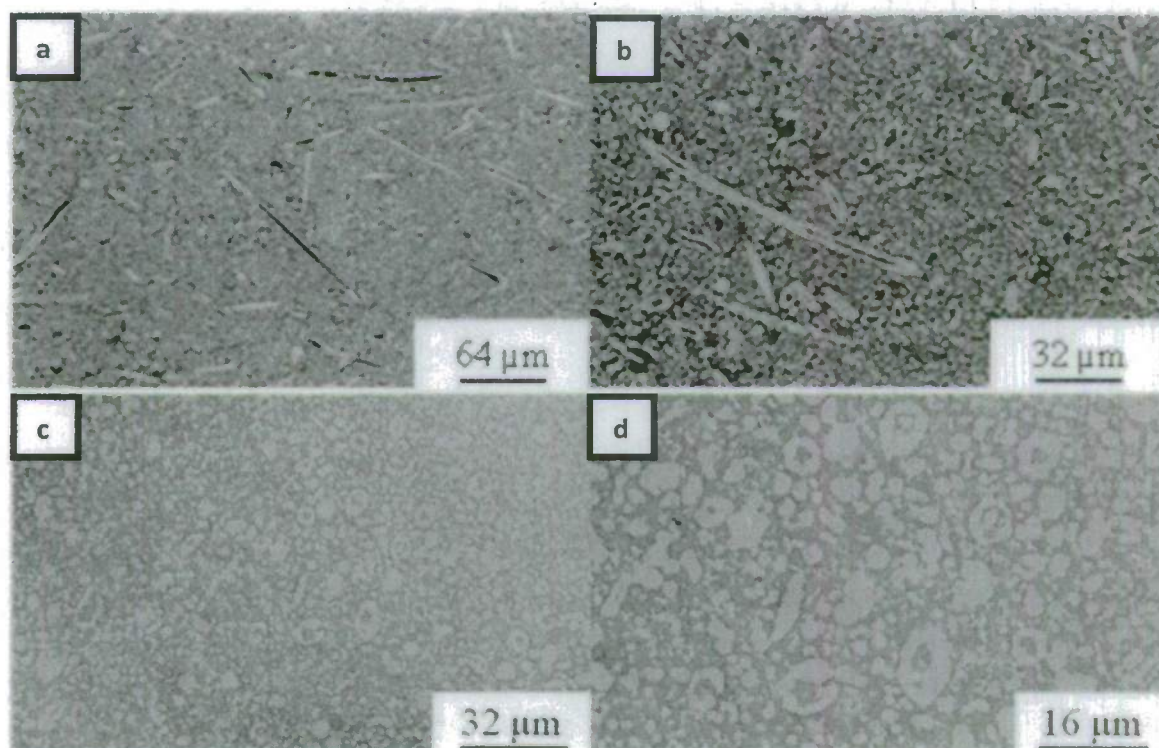

Figure 18. DCP-converted porous WC preforms containing 20 vol. % hollow WC fibers. The preforms were prepared by pressing mixtures of WC powder and hollow WC fibers. Images are shown of cross-sections oriented: (a), (b) parallel to the preform pressing direction and (c), (d) perpendicular to the pressing direction.

V. Kinetics of Reaction Between Molten Hf-Cu and Solid WC

(as reported in: Liu, Y., Lipke, D.W., Zhang, Y. and Sandhage, K.H. "The kinetics of incongruent reduction of tungsten carbide via reaction with a hafnium-copper melt," *Acta Mater.*, 57(13), 3924-3931 (2009).)

The kinetic mechanism of incongruent reduction of WC by reaction with a Hf-Cu melt (to yield W and HfC products) has also been examined. The rate of such incongruent WC reduction has been examined by immersing dense, polycrystalline WC plates in a vertical orientation in

Hf-Cu melts at 1150°C to 1300°C for 1 to 24 h. A tungsten layer of uniform thickness was found to form adjacent to the tungsten carbide, whereas an irregular, but generally continuous hafnium carbide layer formed adjacent to the tungsten layer. The rate of WC reaction was evaluated by measuring the thickness of the W layer as a function of reaction time, temperature, and vertical position along the WC surface. Such kinetic data and microstructural analyses indicated that the incongruent reduction of WC in molten Hf-Cu was controlled by solid-state diffusion, with the likely rate-limiting step being the diffusion of carbon through the W and/or HfC layers.

The incongruent reduction of WC occurred by the following net displacement reaction with an Hf-Cu melt at 1150-1400°C:

$$\{Hf\} + WC \leftrightarrow W + HfC \tag{1.11}$$

where {Hf} denotes Hf dissolved in the Hf-Cu melt. This reaction is highly favored from a thermodynamic standpoint. For example, using available data for the thermodynamic activity of hafnium in Hf-Cu melts[62], along with the standard Gibbs free energies of formation of HfC and WC[24], the Gibbs free energy change associated with the reaction of a 35 at.% Hf melt with WC to yield HfC and W at 1350°C was calculated to be -184.6 kJ/mol.

The steady-state rate of incongruent reduction of WC was examined by using sufficient starting amounts of the reactants, {Hf} and WC(s), so as to avoid significant depletion of these constituents over the course of each experiment. For example, even after 24 h of reaction at 1300°C (the most extreme conditions used in the present work), less than 0.1 at% of the Hf present in the melt and less than 1.1 at. % of the carbon present in the planar WC specimen were consumed to form the W and HfC product layers. The steady-state product morphology at the WC/melt interface (**Figure 19**) consisted of a HfC layer of irregular thickness adjacent to the melt, and a W layer of more uniform thickness that separated the HfC layer from the WC specimen.

Such conformal HfC and W layer formation on WC during reaction with $Zr_2Cu(l)$ may be considered to be an example of *passive incongruent reduction*, by analogy to "passive corrosion" (which generally refers to the formation of a continuous, adherent, solid product layer or layers on a corroding solid surface that act to reduce the rate of corrosion by physically separating the corroding solid from the reactive fluid). However, at certain locations where the HfC layer was not continuous, the rate of consumption of the WC was locally enhanced (i.e., a pit formed), and the exposed W layer reacted with the Hf in the melt to form particles of W_2Hf (**Figure 20**). The accelerated reaction associated with the formation of discontinuous (and apparently less protective) HfC and W_2Hf products may be considered to be an example of *active incongruent reduction* (by analogy to "active corrosion"). Given the non-uniformity in the thickness of the HfC product layer, the thickness of the W layer was used to evaluate the extent of WC consumption after reaction for any particular temperature and time.

The tungsten product layer formed during the passive incongruent of WC was found to thicken at a parabolic rate with time at each reaction temperature from 1150-1300°C (**Figure 21**). Such steady-state parabolic kinetics were consistent with a diffusion-controlled process. If liquid phase diffusion was the rate-limiting step, then the selective removal of hafnium from the melt by reaction (1.12) should have resulted in a gradient in the hafnium concentration of the melt near the melt/WC interface. Such a hafnium concentration gradient should, in turn, have resulted in a gradient in melt density that would lead to convection in the melt near the melt/WC interface. A liquid phase diffusion-controlled process involving such density-driven free convection of the melt past the vertical plate-shaped WC specimen should have led to a steady-state reaction rate that was independent of time, but dependent on vertical position.[63,64] However,
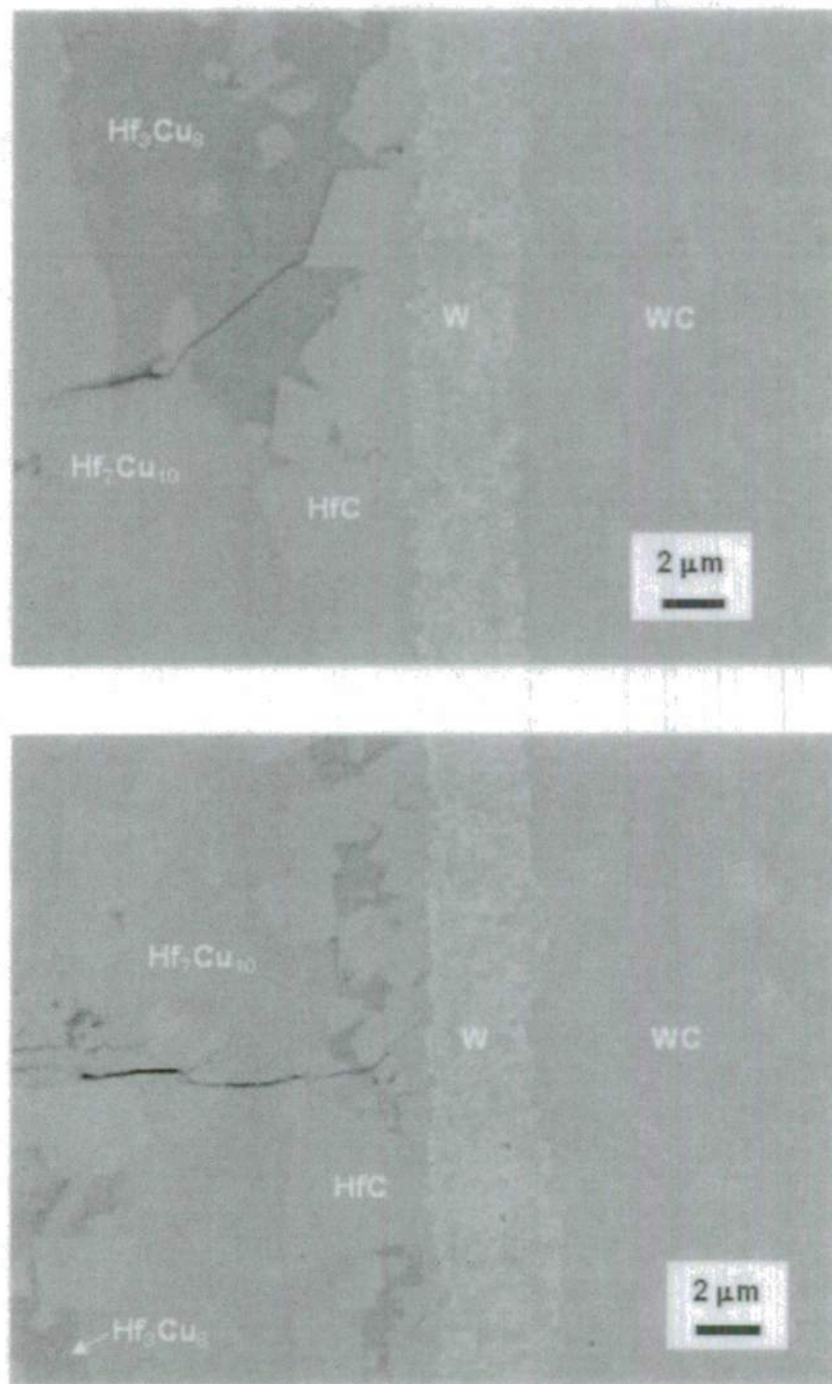
Figure 19. Backscattered electron images of a polished cross-section of the WC/Hf-Cu melt interface obtained after immersion of a dense WC specimen in a Hf-Cu melt at 1300°C for 24 h.
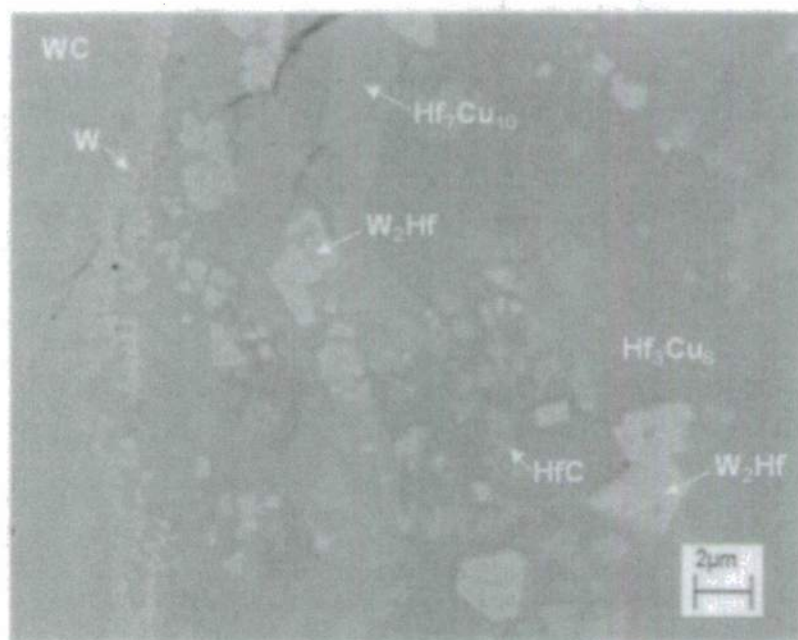
Figure 20. A backscattered electron image of a polished cross-section of the WC/Hf-Cu melt interface obtained after immersion of a dense WC specimen in a Hf-Cu melt at 1200°C for 6 h. Occasional disruptions in the continuity of the HfC layer yielded pits on the WC surface at which a thinner W layer and particles of W_2Hf were detected.
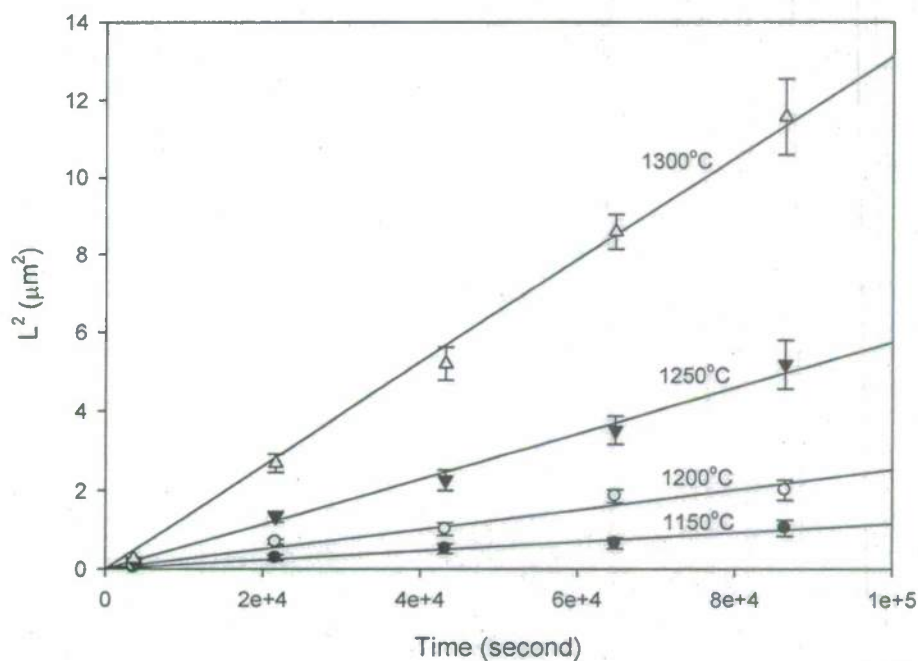

Figure 21. A plot of the square of the average tungsten layer thickness, L^2, vs. immersion time at various reaction temperatures. The lines were generated by least square fitting of the L^2 vs. time data. The error bars indicate the span of $\pm$ one standard deviation about the average value.

the present results indicated that the product layer thickening rates were dependent on time (**Figure 21**) and independent of position (**Figure 22**).
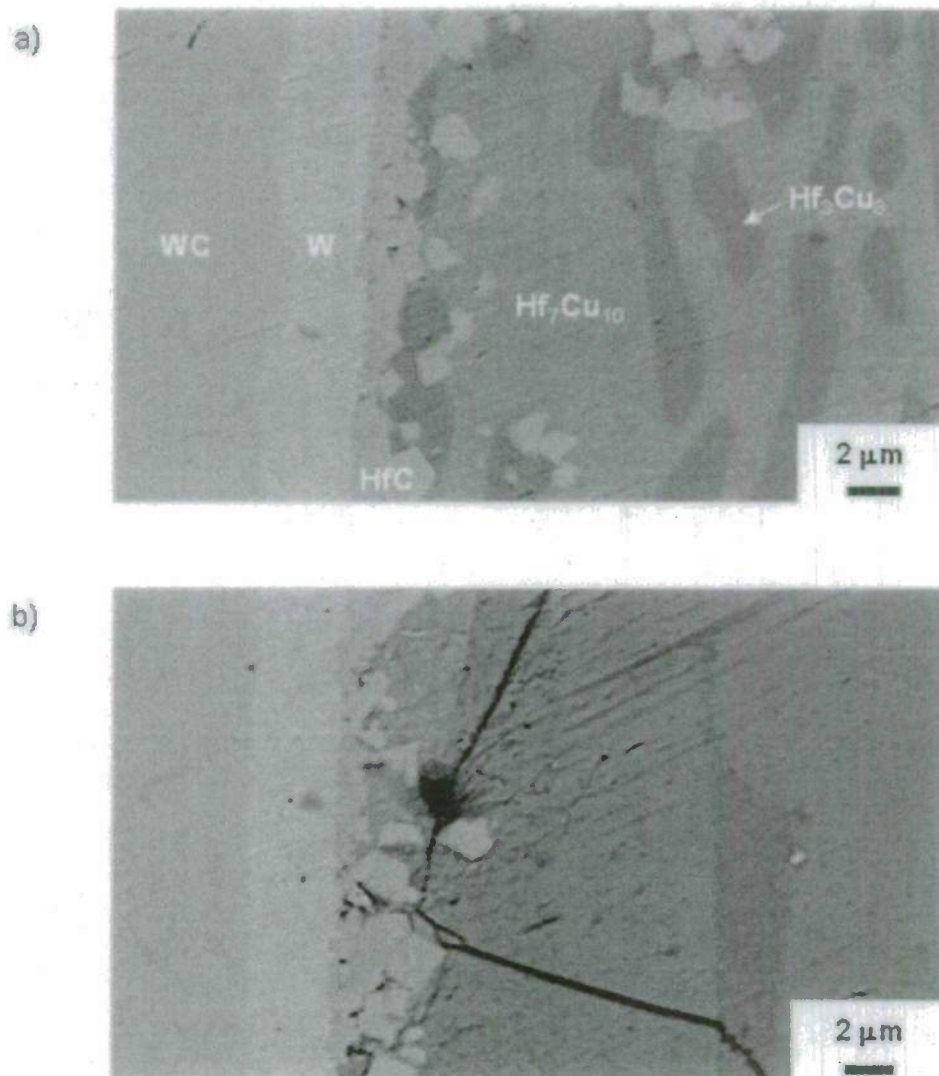

Figure 22. Backscattered electron images of polished cross sections of the WC/Hf-Cu melt interface obtained after immersion of a dense WC specimen in a Hf-Cu melt at 1300°C for 24 h. These cross-sections were obtained at locations: a) within 100 μm of the melt surface (near the top region of the immersed specimen) and b) within 100 μm of the immersed bottom of the WC specimen.
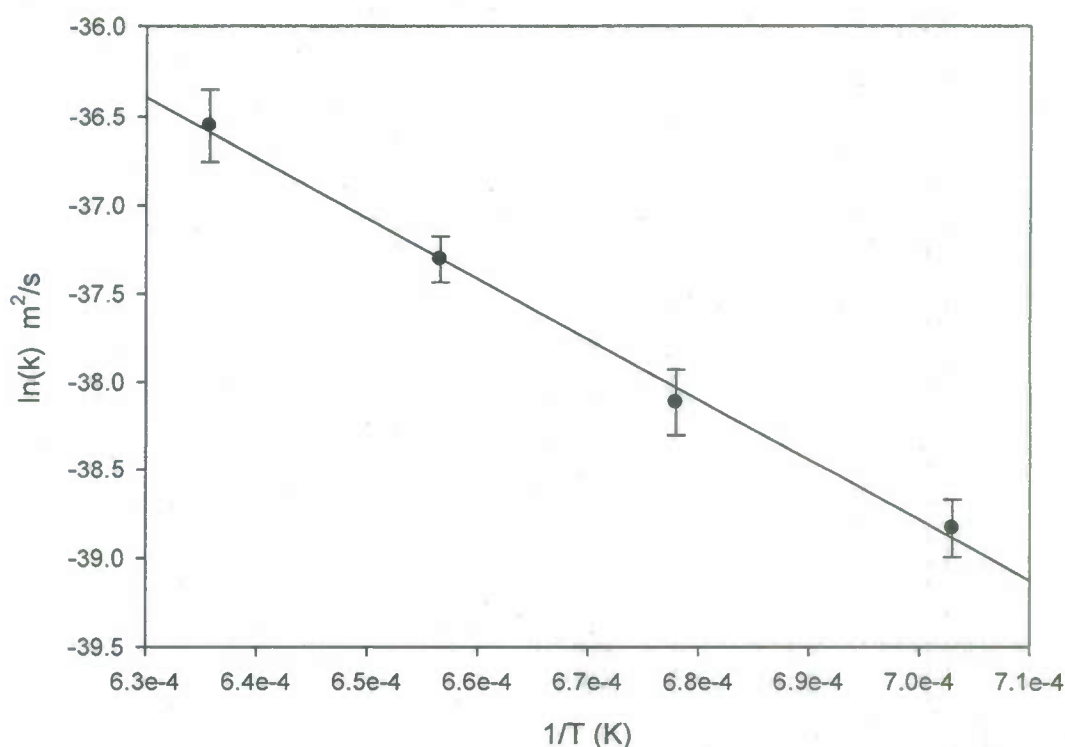
Figure 23. A plot of the logarithm of the parabolic rate constant (for the thickening of the tungsten product layer) vs. the inverse of reaction temperature.

The temperature dependence of the rate of tungsten layer thickening was found to follow Arrhenius behavior (**Figure 23**) with an activation energy of 284 kJ/mol. This value was much higher than has been reported for the diffusion of copper and other group IVB elements (Zr, Ti) in molten copper or molten copper alloys.[65-67] Hence, mass transport through the liquid is unlikely to be the rate-limiting step. Instead, the parabolic growth of the tungsten product layer was consistent with a solid-state diffusion controlled process, such as mass transport through the tungsten carbide specimen, the hafnium carbide product layer, and/or the tungsten product layer. The activation energy reported for the grain boundary diffusion of C through WC by Buhsmer and Crayton (297 kJ/mole[68]) agrees reasonably well with the activation energy observed for the thickening of the W layer in this work (284 kJ/mole). However, at locations where the HfC layer was not continuous, the WC was observed to undergo an enhanced rate of reaction (i.e., a pit formed). Within such pits, the thickness of the tungsten layer was locally reduced and discrete particles of W_2Hf formed. Such enhanced local reaction (pitting) should not have occurred if carbon diffusion through the tungsten carbide was rate limiting; that is, the continuity of the HfC should not have affected the local corrosion rate, if diffusion through the underlying WC was rate limiting. Although no data could be found in the literature for hafnium diffusion through hafnium carbide, the activation energy reported for the lattice diffusion of zirconium through zirconium carbide (a carbide with a similar crystal structure as hafnium carbide) is quite large (719 kJ/mol[69]). Furthermore, prior work[70] has indicated that the formation of a continuous HfC product layer on C undergoing reaction with Hf liquid was controlled by the diffusion of C through the HfC layer (i.e., not by the diffusion of Hf through the HfC layer). The activation energy for the lattice diffusion of carbon through hafnium carbide (545 kJ/mole[71]) is

significantly higher than the value of 284 kJ/mole obtained in the present work. However, diffusion data for the transport of carbon along grain boundaries in hafnium carbide is lacking. The activation energies for grain boundary transport of carbon through titanium carbide[72] and zirconium carbide[73] were significantly lower than for the lattice diffusion of carbon through these carbides. The activation energies reported for carbon diffusion through the lattice of tungsten (224 kJ/mole[74] and 207 kJ/mole[75]) are relatively close to the value of 284 kJ/mole obtained in the present work. Hence, the rate-limiting step for the passive incongruent reduction of tungsten carbide is likely to be the solid-state diffusion of carbon through the lattice of the tungsten product layer and/or through grain boundaries in the hafnium carbide product layer.

References

1. Evans, A. G. and Marshall D. B. "The mechanical behavior of ceramic matrix composites." *Acta Metall.*, **37** (10) 2567-2583 (1989).
2. Chawla, N. and Shen, Y. "Mechanical behavior of particle reinforced metal matrix composites." *Adv. Eng. Mater.*, 3 (6) 357-370 (2001).
3. Speyer, F. "Ablative composites containing in situ reaction-formed refractory metal carbides," *Ind. Eng. Chem. Prod. Res. Develop.*, **10** (1) 99-111 (1971).
4. Raddatz, O., Schneider, G. A., Mackens, W., Voss, H. and Claussen, N. "Bridging stresses and R-curves in ceramic/metal composites," *J. Euro. Ceram. Soc.*, **20** (13) 2261-2273 (2000).
5. Song, G. M., Wang, Y. J. and Zhou, H. "Elevated temperature ablation resistance and thermophysical properties of tungsten matrix composites reinforced with ZrC particles." *J. Mater. Sci.*, **36**, 4625-4631 (2001).
6. Hebsur, M. G. "Development and characterization of $SiC(f)/MoSi_2$-$Si_3N_4(p)$ hybrid composites," *Mat. Sci. Eng.*, A261, 24-37 (1999).
7. Fauchais, P. "Understanding plasma spraying," *J. Phys. D: Appl. Phys.*, **37**, R86-R108 (2004).
8. Patterson, M. C. L., He, S., Fehrenbacher, L. L., Hanigofsky, J. and Reed, B. D. "Advanced HfC-TaC oxidation resistant composite rocket thruster," *Mat. Manu. Proc.*, **11** (3) 367-379 (1996).
9. Chiang, Y. M., Haggerty, J. S., Messner, R. P. and Demetry, C. "Reaction-based processing methods for ceramic-matrix composites," *Am. Ceram. Soc. Bull.*, 68(2), 420-428 (1989).
10. Hozer, L., Lee, J. R. and Chiang Y. M. "Reaction-infiltrated, net-shape SiC composites," *Mat. Sci. Eng.*, **A195**, 131-143 (1995).
11. Sandhage, K. H. "Materials 'alchemy': shape-preserving chemical transformation of micro-to-macroscale 3-D structures," *JOM*, **62** (6) 32-43 (2010).
12. Sandhage, K. H. and Kumar, P. "Method for Fabricating Shaped Monolithic Ceramics and Ceramic Composites through Displacive Compensation of Porosity, and Ceramics and Composites made Thereby," *U. S. Patent No. 6,833,337*, December 21, 2004.
13. Sandhage, K. H., Unocic, R. R., Dickerson, M. B., Timberlake, M., and Guerra, K., "Method for Fabricating High-Melting, Wear-Resistant Ceramics and Ceramic Composites at Low Temperatures, *U.S. Patent No. 6,598,656*, July 29, 2003.
14. Sandhage, K. H. and Kumar, P. "Method for Fabricating Shaped Monolithic Ceramics and Ceramic Composites through Displacive Compensation of Porosity, and Ceramics and Composites made Thereby," *U. S. Patent No. 6,407,022*, June 18, 2002.
15. Kumar, P. and Sandhage, K.H. "The displacive compensation of porosity (DCP) method for fabricating dense, shaped, high-ceramic bearing bodies at modest temperatures," *J. Mater. Sci.*, **34**, 5757-5769 (1999).
16. Dickerson, M.B. et al. "Near net-shape, ultra-high melting, recession-resistant ZrC/W-based rocket nozzle liners via the displacive compensation of porosity (DCP) method," *J. Mater. Sci.*, **39**, 6005-6015 (2004).
17. Thakre, P. and Yang, V. Chemical erosion of refractory-metal nozzle inserts in solid-propellant rocket motors. *J. Propul. Power*, **25** (1) 40-50, (2009).
18. Sutton, G. P. *Rocket propulsion elements*, New York, NY: John Wiley & Sons, 1992, p. 483-488.

19. Arias, D. and Abriata, J.P. Cu-Zr Phase Diagram, ASM Alloy Phase Diagrams Center, P. Villars (ed.), Materials Park, OH: ASM International, (2006).

20. Eremenko, V.N., Velikanova, T.Y., Artyukh, L.V., Aksel'rod, G.M. and Vishnevskii, A.S. *Dopov. Akad. Nauk Ukr. RSR, Ser. A: Fiz.-Mat. Tekh. Nauki*, 1, 80-85 (1976). From Phase Diagrams for Zirconium and Zirconia Systems, H. M. Ondik and H. F. Mcmurdie (ed.), American Ceramic Society, 2005.

21. Kuz'ma, Y.B., Federov, T.F. and Shvets, E.A. "Phase equilibria in the system Zr-W-C," *Porosh. Met.*, **2** (26) 22-25 (1965).

22. Touloukian, Y.S., Kirby, R.K., Taylor, R.E. and Desai, P.D. *Thermophysical Properties of Matter*. Vol. 12: Thermal Expansion of Metallic Elements and Alloys" New York: Plenum Press, (1975).

23. Touloukian, Y.S., Kirby, R.K., Taylor, R.E. and Desai, P.D. *Thermophysical Properties of Matter*. Vol. 13: Thermal Expansion of Non-Metallic Solids" New York: Plenum Press, (1975).

24. Barin, I. *Thermochemical Data of Pure Substances*. Weinheim, Germany: VCH Verlagsgesellschaft, (1995).

25. "JCPDS X-ray Diffraction Card File" Newton Square, PA: International Centre for Diffraction Data, (2010).

26. Storms, E.K. *The Refractory Carbides*. New York: Academic Press, (1967).

27. Lassner, E. and Schubert, W.D. *Tungsten: Properties, Chemistry, and Technology of the Element, Alloys, and Chemical Compounds*. New York: Plenum Publishers, (1999).

28. Grzesik, Z., Dickerson, M. B., and Sandhage, K. H. "The Incongruent Reduction of Tungsten Carbide by a Zirconium-Copper Melt," *J. Mater. Res.*, **18** (9) 2135-2140 (2003).

29. Becher, P.F. "Microstructural design of toughened ceramics," *J. Am. Ceram. Soc.*, **74** (2) 255-269 (1991).

30. Faber, K.T. and Evans, A.G. "Crack deflection processes - I. Theory," *Acta Metall.*, **31** (4) 565-576 (1983).

31. Evans, A.G. and Marshall, D.B. "The mechanical-behavior of ceramic matrix composites," *Acta Metall.*, **37** (10) 2567-2583 (1989).

32. Honjo, K. and Shindo, A. "Carbon fibers with duplex metal carbide coating and methods for manufacture thereof" *U.S. Patent No. 4,405,685* (Sept. 20, 1983).

33. Bouix, et al. "Process for coating carbon fibers with a carbide, and carbon fibers thus coated" *U.S. Patent No. 4,859,503* (Aug. 22, 1989). Continued in part by *U.S. Patent No. 4,921,725* (May 1, 1990).

34. Lennartz, J. W. "Fluidized bed reactor and method for forming a metal carbide coating on a substrate containing graphite or carbon," *U.S. Patent No. 5,498,442* (Mar. 12, 1996).

35. Hamling, B. H. "Process for producing metal carbide fibers, textiles and shapes" U.S. Patent 3403008 (Sept. 24, 1968). Continued in part by *U.S. Patent No. 4,162,301* (July 24, 1979).

36. Gilbert, T. R., Soman, R. S., and Li, J. "Method of forming a carbide on a carbon substrate" *U.S. Patent No. 5,141,773* (Aug. 25, 1992). Continued in part by *U.S. Patent No. 5,238,711* (Aug. 24, 1993).

37. Preiss, H., Meyer, B. and Olschewski, C. "Preparation of molybdenum and tungsten carbides from solution derived precursors," *J. Mater. Sci.*, **33**, 713-722 (1998).

38. Kurokawa, Y., Kobayashi, S., Suzuki, M., Shimazaki, M. and Takahashi, M. "Preparation of refractory carbide fibers by thermal decomposition of transition metal (Ti, Zr, Hf, Nb, Ta) alkoxide-cellulose precursor gel fibers," *J. Mater. Res.*, **13** (3) 760-765(1998).

39. Gadiou, R., Serverin, S., Gibot, P. and Vix-Guterl, C. "The synthesis of SiC and TiC protective coatings for carbon fibers by the reactive replica process," *J. Euro. Ceram. Soc.*, **28**, 2265-2274 (2008).

40. Li, X. et al. "Preparation of a titanium carbide coating on carbon fiber using a molten salt method," *Carbon*, **46**, 305-309 (2008).

41. Nieh, T.G . and Vidoz, A. E. "Carbide coatings on graphite fibers by liquid metal transfer agent method," *J. Am. Ceram. Soc.*, **65** (5) 227-230 (1982).

42. Himbeault, D. D., Varin, R. A. and Piekarski, K. "Coating of graphite fibers with tungsten carbide using solid and liquid copper as a transfer medium," *Met. Trans.*, **19A**, 2109-2113 (1988).

43. Givargizov, E. I. "Fundamental aspects of VLS growth," *J. Cryst. Growth*, 31, 20-30 (1975).

44. Guha, S., Kyriacou, C., Withers, J., Loutfy, R. and Dowding, R. "A low cost synthesis technique for tungsten whiskers of <100> orientation," *Mater. Manu. Proc.*, **9** (6) 1061-1086 (1994).

45. Wang, S. et al. "Formation and growth mechanism of tungsten oxide microtubules," *Chem. Phys. Lett.*, **427**, 350-355 (2006).

46. Bamberger, C. E. "The pseudomorphic conversion of acicular crystals of sodium tungsten bronze into WC/W," *J. Mater. Sci. Lett.*, **13**, 1742-1745 (1994).

47. Byrne, C. E. & Nagle, D. C. Carbonization of wood for advanced materials applications. *Carbon*, **35** (2) 259-266 (1997).

48. Greil, P. Biomorphic ceramics from lignocellulosics. *J. Euro. Ceram. Soc.*, **21** (2) 105-118 (2001).

49. Zakhidov, A. A., et al. Carbon structures with three-dimensional periodicity at optical wavelengths. *Science*, **282**, 897-901 (1998).

50. Adelhelm, P., et al. Generation of hierarchical meso- and macroporous carbon from mesophase pitch by spinodal decomposition using polymer templates. *Adv. Mater*, **19**, 4012-4017 (2007).

51. Besmann, T. M., Sheldon, B. W., Lowden, R. A. and Stinton, D. P. Vapor-phase fabrication and properties of continuous-filament ceramic composites. *Science*, **253**, 1104-1109 (1991).

52. Ledoux, M., Guille J., Pham-Huu, C. and Marin, S. "Production of heavy metal carbides of high specific surface area" *U.S. Patent No. 5,391,524* (Feb. 21, 1995).

53. Paccaud, O. and Derre, A. "Silicon carbide coating by reactive pack cementation - Part I: Silicon carbide/silica interaction," *Chem. Vap. Dep.*, **6** (1) 33-40, (2000).

54. Barin, I. *Thermochemical data of pure substances*, Wiley-VCH (2004).

55. Levin, E. M., Robbins, C. R. and McMurdie, H. F (eds.). *Phase Diagrams for Ceramists: Volume I – Oxides and Salts*. Materials Park, OH: American Ceramic Society (1981).

56. Levin, E. M. "System B_2O_3-WO_3," *J. Am. Ceram. Soc.*, **48** (9) 491-492 (1965).

57. Meulencamp, E. A. "Mechanism of WO_3 electrodeposition from peroxy-tungstate solution," *J. Electrochem. Soc.*, **144** (5) 1664-1671 (1997).

58. Turkdogan, E. T., Grieveson, P. and Darken, L. S. "Enhancement of diffusion-limited rates of volatilization of metals," *J. Phys. Chem.*, **67**, 1647-1654 (1963).

59. Sharafat, S., et al. Ultra-low pressure drop helium-cooled porous-tungsten PFC. *Fusion Sci. & Tech.*, **52**, 559-565 (2007).

60. Dandliker, R. B., Conner, R. D. & Johnson, W. L. Melt infiltration casting of bulk metallic-glass matrix composites. *J. Mater. Res.*, **13**(10), 2896-2901 (1998).
61. Fleming, J. G., Lin, S. Y., El-Kady, I., Biswas, R. and Ho, K. M. All-metallic three-dimensional photonic crystals with a large infrared bandgap. *Nature*, **417**, 52-55 (2002).
62. Berezutski, V. V. and Ivanov, M. I. "Thermodynamics of binary liquid Cu-Hf alloys," *J. Alloys Compounds*, 306, L1-L2 (2000).
63. Wagner, C. "The dissolution rate of sodium chloride with diffusion and natural convection as rate-determining factors," *J. Phys. Colloid Chem.*, 53(7), 1030-1033 (1949).
64. Cooper, A. R. and Kingery, W. D. "Dissolution in ceramic systems. 1. Molecular diffusion, natural convection, and forced convection studies of sapphire dissolution in calcium aluminum silicate," *J. Am. Ceram. Soc.*, 47(1), 37-43 (1964).
65. Henderson, J. and Yang, L. "Self diffusion of copper in molten copper," *Trans. Met. Soc. AIME*, 221(1), 72-73 (1961).
66. Shurygin P. M. and Shantarin, V. D. "Compensation effect in diffusion of metals in molten copper," *Russ. J. Phys. Chem.*, 42(2), 242-243 (1968).
67. Gaukel, C., Kluge, M. And Schober, H. R. "Diffusion mechanisms in under-cooled binary liquids of $Zr_{67}Cu_{33}$," *J. Non-Cryst. Solids*, 664(Part 2), 250-252 (1999).
68. Buhsmer, C. P. and Crayton, P. H. "Carbon self diffusion in tungsten carbide," *J. Mater. Sci.*, 6(7), 981-988 (1971).
69. Andrievskii, R. A., Khromov Y. F. and Alekseeva, I. S. "Self-diffusion of carbon and metallic atoms in zirconium and niobium carbides," *Fiz. Metal. Metalloved.*, 32(3), 664-667 (1971).
70. Adelsberg, L. M. and Cadoff, L. H. "Reactions of liquid titanium and hafnium with carbon," *Trans. Met. Soc. AIME*, 239(6), 933-935 (1967).
71. Andrievskii, R. A., Klimenko, V. V. and Khromov, Y. F. "Self-diffusion of carbon in groups IV and V transition-metal carbides," *Fiz. Metal. Metalloved.*, 28(2), 298-303 (1969).
72. Albertsen, K. and Schaller, H. J. "Diffusion of carbon in titanium carbide," *Berich. Bunsen Gesell.*, 98(10), 1224-1230 (1994).
73. Sarian, S. and Criscione, J. M. "Diffusion of carbon through zirconium monocarbide," *J. Appl. Phys.*, 38(4), 1794-1798 (1967).
74. Nakonechnikov, A. I., Pavlinov, L. V. and Bykov, V. N. "Diffusion of carbon in refractory metals with a BCC lattice," *Fiz. Metal. Metalloved.*, 22(2), 234 (1966).
75. Aleksandrov, L. N. and Shelkonogov, V. Y. "Diffusion of carbon in tungsten and molybdenum with low concentration of carbon," *Sov. Powder Metall. Met. Ceram.*, 3, 288-292 (1964).